Catena 208 (2022) 105785

Contents lists available at ScienceDirect

Catena

journal homepage: www.elsevier.com/locate/catena

Tectonic and climatic forcing of chemical weathering intensity in the northeastern Tibetan Plateau since the middle Miocene

Hanjing Fu, Xing Jian *, Hanghai Liang, Wei Zhang, Xiaotian Shen, Ling Wang

State Key Laboratory of Marine Environmental Science, College of Ocean and Earth Sciences, Xiamen University, Xiamen 361102, PR China

ARTICLE INFO

Keywords:
Chemical weathering
Tibetan Plateau
Cenozoic sediments
Paleoclimate
Sediment provenance analysis

ABSTRACT

Chemical weathering of continental silicates is a crucial geological process in regulating Earth's long-term climate and participating in global carbon cycle. The increasing aridity and active tectonic settings in the northeastern Tibetan Plateau since the middle Miocene, combining the global cooling background, make this region ideal for studying how the weathering process interacts with climate and tectonics. We focus on a well-dated Cenozoic sedimentary profile in the northeastern Qaidam Basin and use sandstone petrography, heavy minerals, mudstone clay minerals and geochemical data to interpret sediment provenance and to reconstruct paleo-chemical weathering history (15.3–1.8 Ma) in the northeast Tibet. Our results demonstrate unchanged sediment sources (the South Qilian Shan and the North Qaidam belt) and moderate chemical weathering intensity (CIA values of 67–80) for the sediment source-to-sink system since the middle Miocene. The high chemical weathering intensity in 15.3–12 Ma corresponded to relatively warm and humid climate, indicating minor efforts of global cooling (14–12 Ma) to the local weathering processes. The weakening chemical weathering in 12–9 Ma was closely related to rapid exhumation of the South Qilian Shan and accelerated growth of the northeastern Tibetan Plateau. Uplift-induced enhancement of physical denudation and regional aridity had triggered the transition of chemical weathering regime from supply-limited to kinetic-limited. The inspiring enhanced chemical weathering in 9–6 Ma was attributed to orographic rainfall or intensified East Asian monsoon precipitation. The warm periods and onset of the Northern Hemisphere Glaciation during the Pliocene-Pleistocene controlled the evolution of chemical weathering in the Qaidam Basin. Collectively, we propose that the late Cenozoic chemical weathering intensity in the northeastern Tibet was both constrained by tectonic deformation and climate change. Our findings emphasize the discordance between chemical weathering intensity and climate in arid, tectonically-active regions and thus caution should be exercised while using paleo-weathering intensity to reconstruct paleoclimate history.

1. Introduction

The physical denudation and chemical weathering of continental rocks play important roles in shaping the morphology of Earth's surface and regulating global chemical cycles (Clift et al., 2014; Maher and Chamberlain, 2014; Riebe et al., 2017; Penman et al., 2020). Silicate weathering is considered to be a net carbon sink on geological time scales through consumption and transformation of atmospheric CO_2 to carbonate stored in the oceans (Kump et al., 2000; Oliva et al., 2003; Kasting, 2019). The mechanisms and the controls of continental silicate chemical weathering have received widespread attentions in recent years. Climatic (e.g., temperature and precipitation) and tectonic (e.g., relief, slope and physical denudation) factors are considered to have significant impacts on silicate weathering processes (West et al., 2005; Wan et al., 2012; Yang et al., 2020). The Tibetan Plateau is well known to have experienced a complex deformation history and climatic fluctuations during the Cenozoic (Raymo and Ruddiman, 1992; Guo et al., 2002; Sun and Wang, 2005; Wang et al., 2011; Sun et al., 2014, 2017; Wang et al., 2014; An et al., 2015; Liu et al., 2017). The northeastern Tibetan Plateau, which is far away (>1500–2000 km, Fig. 1) from the India-Asia plate collisional zone with a complex kinematic setting and is currently influenced by both the westerlies and the Asian monsoon, in particular, is an ideal test ground for studying interactive links between climate, tectonics and chemical weathering (Lease et al., 2012; An et al., 2012; Miao et al., 2016b; Fang et al., 2019).

The East Asian summer monsoon (EASM) expanded westward and

* Corresponding author.
E-mail address: xjian@xmu.edu.cn (X. Jian).

https://doi.org/10.1016/j.catena.2021.105785
Received 10 April 2021; Received in revised form 28 September 2021; Accepted 4 October 2021

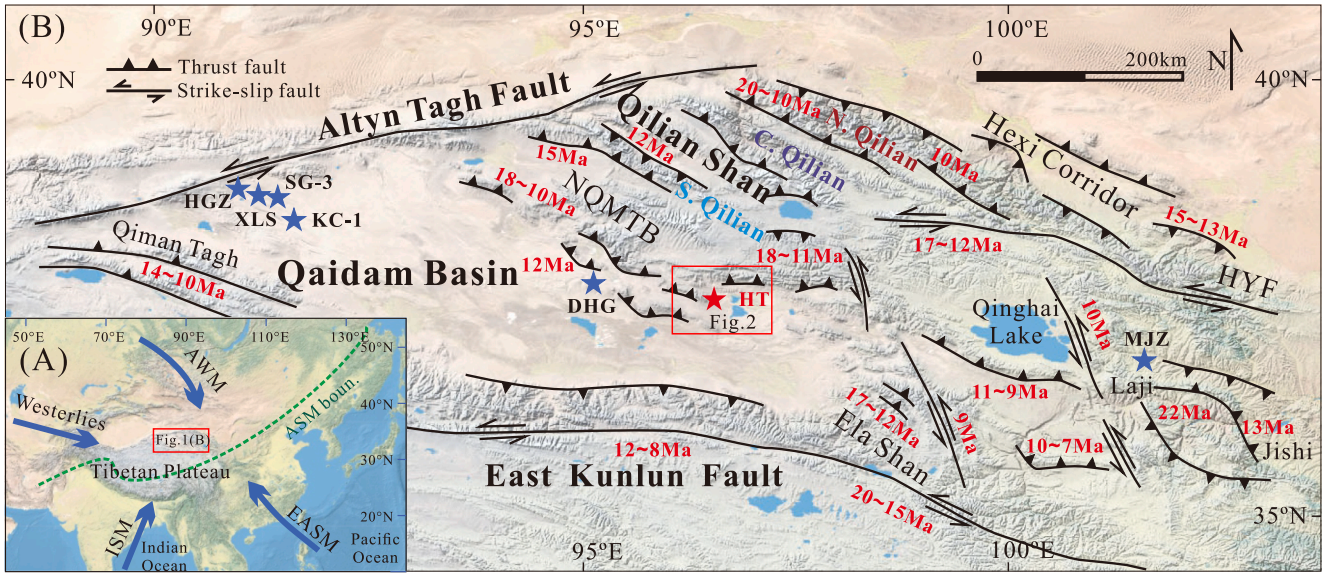

Fig. 1. (a) Location of the Tibetan Plateau and main atmospheric circulation systems (AWM: Asian winter monsoon, ISM: Indian summer monsoon, EASM: East Asian summer monsoon, ASM boun.: modern Asian summer monsoon boundary, after Miao et al. (2016b)). (B) Topographic map of the northeastern Tibetan Plateau with active time of major faults in the late Cenozoic (NQMTB: North Qaidam marginal thrust belt, HYF: Haiyuan Fault). The initiation ages were from references of Zhuang et al. (2018), Yu et al. (2019) and Wang et al. (2020c), which were based on the summary of published sedimentary, magnetostratigraphic and thermochronological evidences. Paired arrows indicate strike-slip faults. Barbed lines are thrust faults. Red star is the research area of this study (HT: Huaitoutala section). Blue stars represent the sections and cores involved in this study. The SG-3 and KC-1 cores were derived from Miao et al. (2013). Sedimentary core in the Xiaoliangshan (XLS) area is referenced from Jian et al. (2014). Dahonggou (DHG) and Honggouzi (HGZ) sections were derived from Sun et al. (2020) and Zhang et al. (2018), respectively. Mojiazhuan (MJZ) section of the Xining Basin was referenced from Zan et al. (2018). (For interpretation of the references to colour in this figure legend, the reader is referred to the web version of this article.)

northward in the Middle Miocene Climatic Optimum (MMCO, 18–14 Ma), covering the Qaidam Basin (Fig. 1) in a warm and humid climate (Miao et al., 2016b). After that, in the context of global cooling, the regional aridity and coldness of the Qaidam Basin were continuously enhanced, which were evidenced by the carbon and oxygen isotope records from several profiles (such as the Dahonggou section and sedimentary cores in the Xiaoliangshan area) (Jian et al., 2014; Sun et al., 2020; Fig. 1), the increased concentration of SO_4^{2-} and Cl^- in the Honggouzi section (Song et al., 2014; Zhang et al., 2018), and the decreased thermophilic and increased xerophytic pollens in KC-1 and SG-3 cores (Miao et al., 2013). The accelerated upward and outward growth of the northeastern Tibetan Plateau since the middle Miocene (<15 Ma) is supported by abundant thermochronological, magnetostratigraphic, sedimentary and paleontological evidences. Specifically, rapid exhumation and extensive crustal deformation occurred in the Qaidam Basin (Fang et al., 2007; Mao et al., 2014; Liu et al., 2017) and surrounding mountains, e.g., Eastern Kunlun Shan (Sun et al., 2008; Duvall et al., 2013), Altyn Tagh (Li et al., 2015; Yu et al., 2019), Qilian Shan (Lu and Xiong, 2009; Zheng et al., 2010; Fang et al., 2013), Laji Shan (Lease et al., 2007), Liupan Shan (Zheng et al., 2006; Wang et al., 2011), Jishi Shan (Lease et al., 2012), Longmen Shan (Xu and Kamp, 2000; Kirby et al., 2002; Godard et al., 2009), as well as the adjacent Guide Basin (Li et al., 2014), Linxia Basin (Fang et al., 2016) and Sichuan Basin (Wang et al., 2012a; Yuan et al., 2013). The regional changes over time in the northeastern Tibetan Plateau indicated by the published results, including poor hydroclimate conditions and intensified tectonic activity, seems to favor weakened chemical weathering intensity since the middle Miocene.

Cenozoic chemical weathering history of the Tibetan Plateau has been reconstructed over different time scales from million years to millennia (e.g., Jian et al., 2013b, 2019; Miao et al., 2016a; Song et al., 2018a; Hu et al., 2019; Zhang et al., 2020). However, the main controlling factor of the late Cenozoic chemical weathering processes in this region remains controversial. Several researches suggest that the global temperature has a primary control on the chemical weathering intensity due to the consistent relationships between marine benthic foraminifera $\delta^{18}O$, sea surface temperature and Chemical Index of Alteration (CIA) (Zachos et al., 2001; Wan et al., 2012; Ren et al., 2020). However, the Miocene sedimentary strata in the Tarim Basin and Linxia Basin reveal an overwhelming tectonic control on the regional chemical weathering intensity (Wang et al., 2016; Yang et al., 2016). Tectonic uplift and deformation are often accompanied by the intensification of physical denudation, shifts of source regions and depocenters, changes of topographic relief and sedimentary environments, causing notable variations in chemical weathering intensity (Filippelli, 1997; Fang et al., 2007; Liu-Zeng et al., 2008; Zhang et al., 2017; Zhu et al., 2017). Additionally, the regional climate change induced by complex tectonics-climate interactions in alpine regions makes it difficult to distinguish the effects of tectonics and climate change on chemical weathering processes (Cheng et al., 2019; Yang et al., 2019). For example, the elevated topography of the northeastern Tibetan Plateau in the late Cenozoic had significantly changed wind regimes to intensify the East Asian monsoons and induced orographic rainfall shadows (Harris, 2006; Clift et al., 2008; Miao et al., 2012; Li et al., 2014; Zhang et al., 2015). The uplift of basin bounding mountains may block moisture and intensify evaporation, resulting in basin interior aridity (Broccoli and Manabe, 1992; Kent-Corson et al., 2009; Shi et al., 2011; Liu et al., 2015; Yang et al., 2017; Guo et al., 2018a). Therefore, studying the evolution and driving mechanism of chemical weathering can help to clarify the geological history of the northeastern Tibetan Plateau and to better understand the interactions between tectonic, climate and chemical weathering processes.

In a word, whether tectonics or climate played the first-order control on the late Cenozoic chemical weathering evolution in the northeastern Tibetan Plateau remains to be answered. This study conducted mudstone bulk mineralogical, clay mineralogical and geochemical analyses from the well-dated Huaitoutala section in the Qaidam Basin (Figs. 1–2), combining sandstone petrographic and heavy mineral data, 1) to evaluate the intensity of paleo-chemical weathering since the middle Miocene, 2) to explore the dominant controlling factors on weathering processes and 3) to better understand the tectonic and

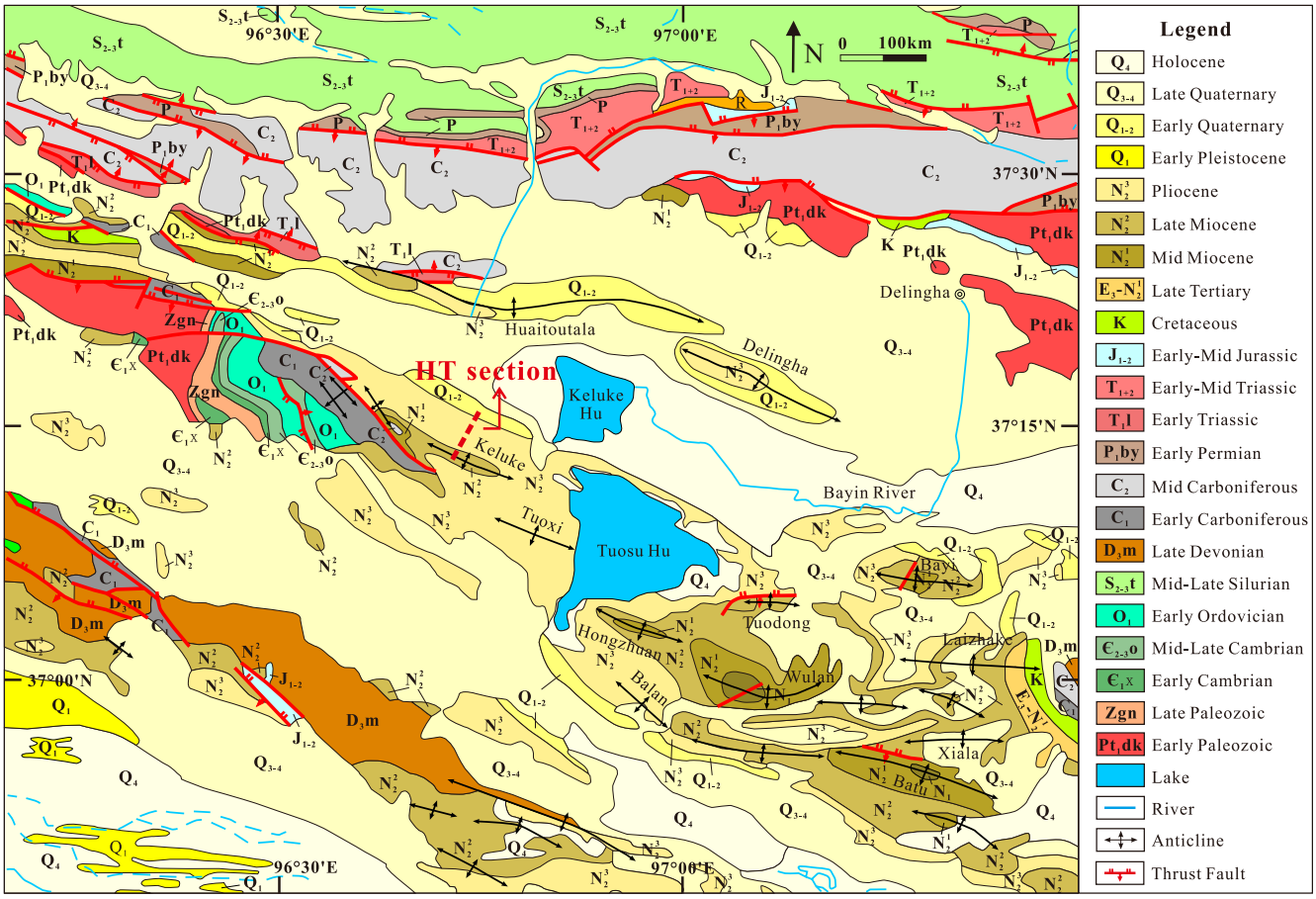

Fig. 2. Geological map of Huaitoutala research area in the northeastern margin of Qaidam Basin, modified from Fang et al. (2007). Red dotted line represents the sampling path (HT section). (For interpretation of the references to colour in this figure legend, the reader is referred to the web version of this article.)

paleoclimatic controls on basin sedimentary records in the northeastern Tibetan Plateau.

2. Geological setting

The Qaidam Basin, covering an area of 120,000 km^2, is the largest intermountain basin in the northeastern Tibetan Plateau (Fig. 1). This basin is bounded by the Eastern Kunlun Shan in the south, by the Qilian Shan in the northeast and by the Altyn Tagh fault in the northwest (Ren et al., 2019; Jian et al., 2020b). The Qilian Shan is mainly composed of the Paleoproterozoic-early Paleozoic metamorphic rocks, the early Paleozoic and Permian-Triassic plutons, volcanic rocks, marine sedimentary rocks and ophiolite sequence (Zhang et al., 2021a). The basement rocks of the Eastern Kunlun Shan primarily consist of the Neoproterozoic-Paleozoic metamorphic rocks and the late Cambrian-Devonian and Permian-Triassic granitoid rocks (Jian et al., 2020b). The Altyn Shan is principally composed of the Proterozoic, Ordovician-Silurian, and Permian igneous and metamorphic basement, as well as the Neoproterozoic quartz arenite and limestone (Bush et al., 2016).

Mesozoic geological evolution of the Qaidam Basin is thought to be closely related to the collision of intra-Eurasian blocks and the subduction of the Tethys Ocean (Ritts and Biffi, 2001; Kapp et al., 2007; Gehrels et al., 2011; Jian et al., 2013b). The late Paleocene-early Eocene Indo-Asian collision (ca. 50–55 Ma) and subsequent convergence resulted in the uplift of Eastern Kunlun Shan, the faults movement and crust shortening in the South Qilian Shan and North Qaidam Basin (Yin et al., 2002; Zhuang et al., 2011a; Bush et al., 2016; Bao et al., 2017). Thermochronological evidences revealed that extensive exhumations of the Altyn Tagh and Eastern Kunlun Shan around the Qaidam Basin during the late Eocene-early Oligocene (Jolivet et al., 2001; Liu et al., 2007a; Clark et al., 2010). The early Oligocene leaf fossils (ca. 30.8 Ma) in the basin indicates that the ground vegetations were at an altitude of 3.3 ± 1.4 km with a temperate and moderately wet climate (Song et al., 2020). The deformation of the Qaidam Basin and the rapid uplift of the surrounding mountains, including the Altyn Tagh (Lu and Xiong, 2009; Lu et al., 2014), Qimen Tagh (Zhou et al., 2018), Eastern Kunlun (Mao et al., 2014) and Qilian Mountains (Nie et al., 2020), occurred in the Miocene (especially 12–8 Ma) (Li et al., 2020 and references therein). Due to the global cooling and regional tectonic forces, the Qaidam Basin had experienced climate change from warm and humid in the MMCO to cold and dry in the late Miocene-Quaternary (Bao et al., 2017, 2019; Miao et al., 2019).

The massive Cenozoic sedimentary succession deposited in the Qaidam Basin with a maximum thickness of 12 km, which records the formation and filling history of the basin and also the tectonic evolution of the adjacent mountains (Yin et al., 2008). The Cenozoic stratigraphy can be divided into six formation units with assigned ages. From oldest to youngest, the lithostratigraphic units are the Lulehe Formation (Fm.) in the Paleocene-Eocene (E_{1+2}), the Xia Ganchaigou Fm. in the Oligocene (E_3), the Shang Ganchaigou Fm. in the early Miocene (N_1), the Xia Youshashan Fm. in the middle Miocene (N_2^1), the Shang Youshashan Fm. in the late Miocene (N_2^2), the Shizigou Fm. in the Pliocene (N_2^3) and the Qigequan Fm. in the early Pleistocene (Q_1) (Fang et al., 2007; Lu and Xiong, 2009; Wang et al., 2012b; Ji et al., 2017).

The Huaitoutala section (abbr: HT section) is located in the northeastern Qaidam Basin (96°43′10″E, 37°13′48″N, Fig. 2), along the north limb of the Keluke anticline in the Delingha Depression (Bao et al., 2019). The well-exposed 4570 m thick Cenozoic deposits in the HT

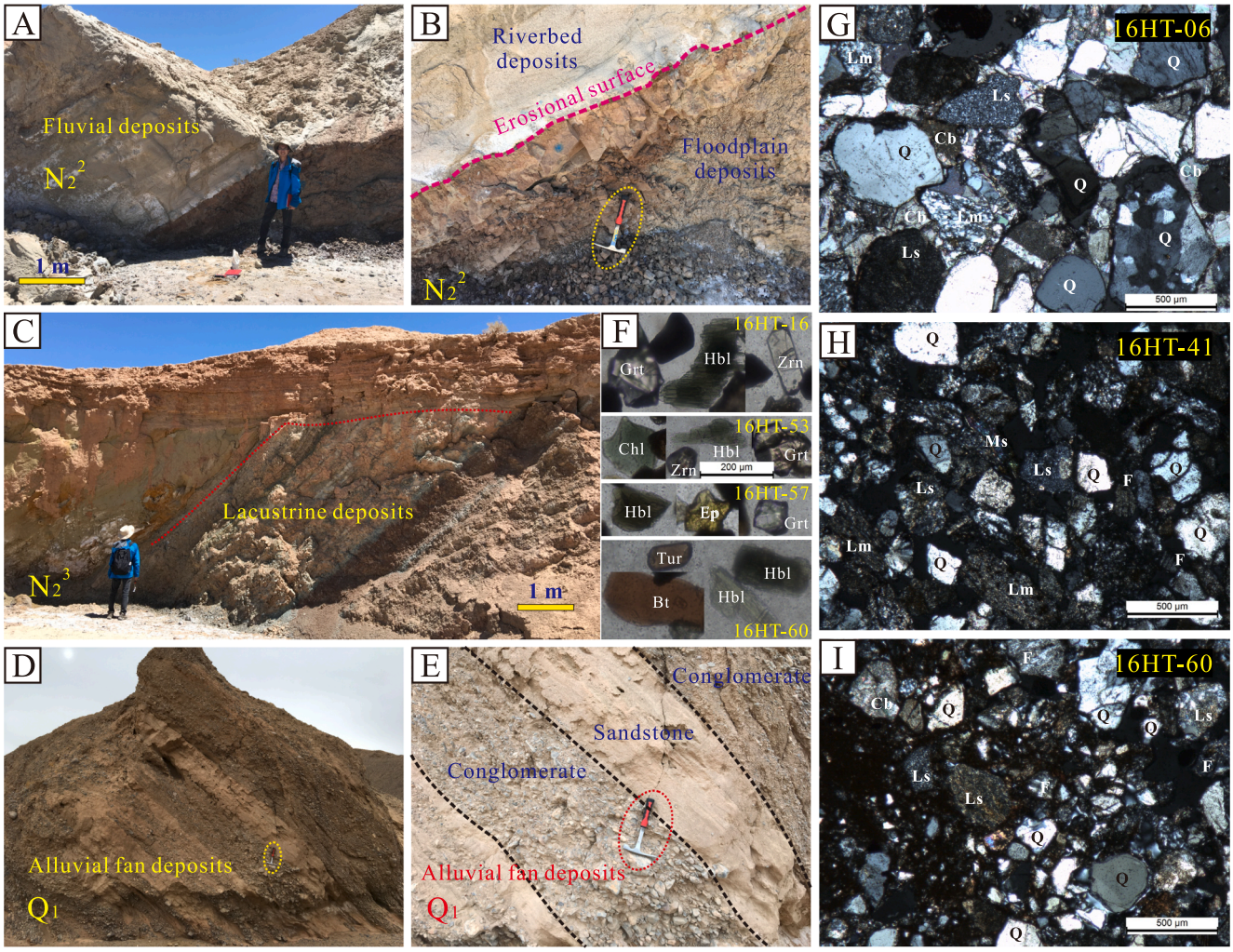

Fig. 3. Field photographs of stratigraphic units and lithofacies at the Huaitoutala section (A–E) and representative microscopic photos of heavy minerals (F) and sandstone petrography (G–I) (orthogonally polarized light). (A–B) Fluvial facies in the Shang Youshashan formation with floodplain (lower part, siltstone and mudstone) and riverbed (upper part, sandstone) deposits divided by the erosional surface. (C) Shallow lacustrine facies in the Shizigou formation with colorful thin-layer fine-grained sediments (gray, gray-green, red-brown). (D–E) Alluvial fan facies in the Qigequan formation with interbedded sandstone and conglomerate. The petrological identification results of sandstones shown here include: (G) 16HT-06 from Shang Youshashan, (H) 16HT-41 from Shizigou and (I) 16HT-60 from Qigequan formations. Sandstones are moderately-poorly sorted and rich in rock fragments, containing slight carbonate debris and calcareous cement. Q: quartz; F: feldspar; Ls: sedimentary lithic fragments; Lm: metamorphic and metasedimentary lithic fragments; Ms: muscovite; Cb: carbonate; Grt: garnet; Hbl: hornblende; Zrn: zircon; Ep: epidote; Tur: tourmaline; Chl: chlorite; Bt: biotite. (For interpretation of the references to colour in this figure legend, the reader is referred to the web version of this article.)

section consist of the upper Xia Youshashan Fm. (100 m), Shang Youshashan Fm. (100–2350 m), Shizigou Fm. (2350–4100 m) and lower Qigequan Fm. (4100–4570 m) with magnetostratigraphic ages ranging from 15.7 to 1.8 Ma (Fang et al., 2007). Although the stratigraphic dating of Cenozoic sedimentary strata in the Dahonggou section is under debate with two age models of ~ 50–7 Ma (Ji et al., 2017) and ~ 25–5 Ma (Wang et al., 2017b)/ ~20–5 Ma (Ren et al., 2019; Nie et al., 2020), there is no objection to the depositional ages of the Huaitoutala section (15.7–1.8 Ma). Sedimentary strata in the HT section were mainly deposited in fluvial-lacustrine sedimentary environments and conformably contact with each other (Zhuang et al., 2011a; Jian et al., 2013b; Bao et al., 2019). The Xia Youshashan Fm. is characterized by brown siltstone, mudstone and marl. The Shang Youshashan Fm. is dominated by yellow-gray conglomerate and sandstone intercalated with siltstone, and the uppermost part mainly consists of mudstone and siltstone. The Shizigou Fm. is mainly characterized by blue-gray sandstone intercalated with calcareous sandy mudstone. The Qigequan Fm. consists of thick gray conglomerate intercalated with thin sandy siltstone and mudstone (Fig. 3A–E; Fang et al., 2007; He et al., 2018; Bao et al., 2019; Ren et al., 2019).

3. Materials and methods

3.1. Samples

In this study, a total of 60 late Cenozoic sedimentary rocks were collected from the HT section (Fig. 4), involving the Shang Youshashan (15.3–8.1 Ma), Shizigou (8.1–2.5 Ma) and Qigequan (<2.5 Ma) formations. Fresh rock samples were collected after stripping the surface layer to avoid the interferences by weathering, pedogenesis and anthropogenic activity. The collected samples mainly consist of mudstones and siltstones with subordinate sandstones, as well as minor paleosols and marls. Detailed information of the field location and sedimentological description of the sampled section can be found in Fig. 2 and Fig. 4. The paleocurrent orientation measurements were conducted based on field observations of cross-stratification sets of sandstones, ripple marks and the orientation distributions of channel sands and gravel imbrications deposited in fluvial environments.

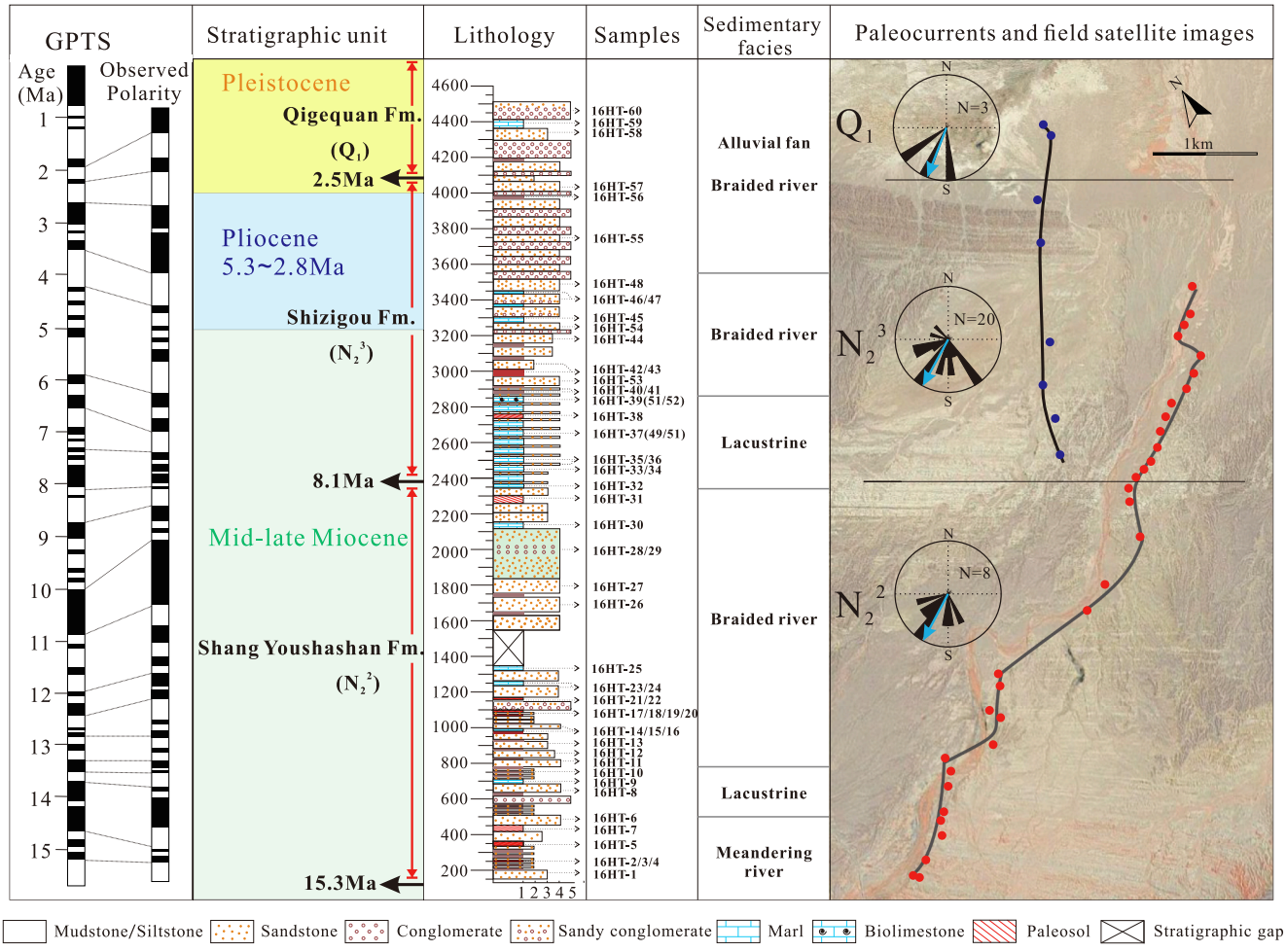

Fig. 4. Comprehensive infographic of magnetostratigraphic chronological and stratigraphic framework (referenced from Fang et al. (2007)), formations, lithologic descriptions, paleocurrents and satellite images (www.earth.google.com) of the Huaitoutala section. The grain size of lithology is divided into five grades, i.e., 1: mud/silt, 2: fine sand, 3: medium sand, 4: coarse sand, 5: conglomerate.

3.2. Petrography

The framework grain compositions and textures recorded the entire source-to-sink sedimentary history and diagenetic process of a clastic sedimentary rock. The information of source rock type, tectonic background, hydrodynamic condition and sedimentary environment can be inferred directly through the results of sedimentary petrography analysis. A total of 15 well-consolidated sandstone samples were cut into standard thin sections. The prepared thin sections were observed under a polarizing microscope to identify the sedimentary textures (grain size, roundness, sorting) and to count the percentages of framework grains (i.e., quartz, feldspar, lithic fragments) by the Gazzi-Dickinson method (Dickinson and Suczek, 1979; Dickinson, 1985). More than 400 points were counted for each sample.

3.3. Heavy mineral analysis

The assemblage of heavy minerals (specific gravity > 2.86) in sandstones has been regarded as a robust indicator for tracing the parent-rock lithology and sediment source to sink process. We selected 10 sandstone samples for transparent heavy mineral analysis. The sandstone samples were preliminarily crushed and 63–250 μm fractions were sieved. The 63–250 μm fractions were weighed for each sample and soaked in 1 mol/L HCl for 24 h to remove carbonate. Heavy minerals were then separated by the tribromomethane ($\rho = 2.89$ g/cm^3) in a separatory funnel. The separated heavy minerals were placed on the glass slides and fixed by Canada balsam. Approximately 200 heavy mineral grains were identified and counted under a polarizing microscope.

3.4. Bulk mineral composition analysis

Bulk mineralogical analysis of 13 mudstone, paleosol and marl samples (ground to powder with grain size < 200 mesh) was carried out by using a Rigaku X-ray diffractometer (XRD) (Ultima IV) at Xiamen University and followed the analytical procedures given by Jian et al. (2019). Each powdered sample was continuously scanned under 40 kV, 30 mA, step width of 0.02°, 2θ range of 5–60° and scanning speeds of 4°/min.

3.5. Clay mineral analysis

A total of 37 mudstone and paleosol samples were simply crushed at first. 3–5 g sample was soaked in deionized water adding 0.05 g $(NaPO_3)_6$ and was dispersed for 30 mins by using an ultrasonic oscillator. The clay fractions (<2 μm) were separated according to the Stoke's law and then concentrated in a centrifuge. And then the clay components were treated with 10% H_2O_2 and 1 mol/L CH_3COOH to remove organic matter and calcium carbonate. The treated particles were placed on the quartz slides, air-dried, for obtaining the oriented mounts. These oriented mounts were then placed in a vacuum pressure box and were saturated with ethylene glycol vapor for 48 h. Each sample

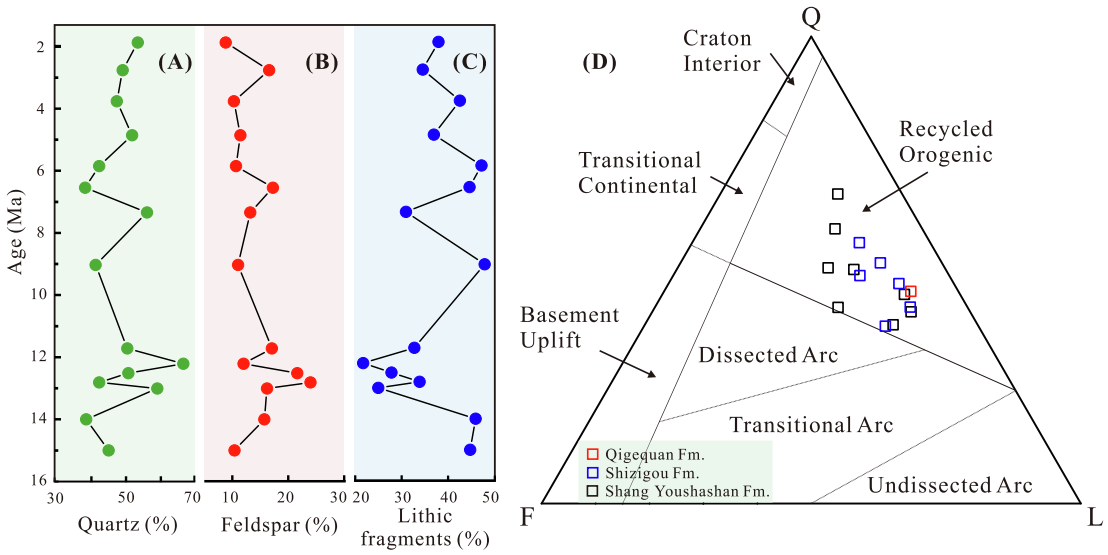

Fig. 5. Variations in the proportion of framework grains ((A) quartz, (B) feldspar and (C) lithic fragments) over time, and (D) the quartz-feldspar-lithics (Q-F-L) plot for provenance discrimination, referenced from Dickinson and Suczek, (1979).

was constantly scanned under 40 kV and 40 mA by using a Rigaku X-ray diffractometer (Ultima IV) with the 2θ range of 3°–35°, speed of 4°/min and step width of 0.02°.

Relative percentages of clay minerals were semi-quantitatively estimated by identifying the basal reflection peak areas of the smectite (17 Å), illite (10 Å), kaolinite (7.2 Å) and chlorite (7.1 Å) peaks (Moore and Reynolds, 1997; Wang et al., 2017a; Song et al., 2018b; Liu et al., 2020). Illite crystallinity index (KI) (Ehrmann, 1998) was measured as the full width at half maximum (FWHM) of the (0 0 1) peak of illite (10 Å) (Alizai et al., 2012). Illite chemistry index (CI) was calculated based on the ratio of the basal reflection peak area of illite 5 Å (0 0 2) and 10 Å (0 0 1) peaks (Esquevin, 1969). All the treatment and data interpretation procedures are also reported by Mei et al. (2021).

3.6. Major-, trace- and rare earth element geochemistry

We selected 33 fine-grained samples (mudstone and siltstone) for major element geochemistry analysis and 5 therein for trace and rare earth element (REE) analysis. Each sample was firstly ground into powers with grain size < 200 mesh and was treated with 1 mol/L CH_3COOH and 10% H_2O_2 solution for 24 h to remove calcium carbonate and organic matter. The concentrations of major elements were obtained by an X-ray fluorescence (XRF) spectrometer (AB-104 L, PW2404) following the method of Hu et al. (2019). Each 0.4 g powered sample was adequately stirred in Ni-pots with anhydrous $Li_2B_4O_7$, 120 mg/ml NH_4Br and suitable oxidant. And then the Ni-pots were put on the CLAISSIE sampling machine for liquefaction. Finally, the well-mixed melt was cooled and dried for XRF analysis. Trace and rare earth elements analysis was performed by an ICP-MS (Agilent 7900). Analytical procedures were following Guo et al. (2018b) and Jian et al. (2020a). The sample powders were accurately weighed (25 mg) and were digested with 1 ml HNO_3 and 3 ml HF for 24 h in a Teflon vessel and heated on a hot plate at 150 ℃ to evaporate. The near-dry solution was digested again with the mixed HNO_3-HF. After further drying, 4 ml HNO_3 were added to the sample and heated for 24 h and then the solution was diluted with 2% HNO_3 for determination. The accuracy and precision of element analysis are better than 5%.

4. Results

4.1. Paleocurrent orientations

The paleocurrent orientation results were plotted as rose diagrams in Fig. 4, indicating almost consistent southwest-directed paleo-flows in the HT section since the middle Miocene, except the minority of southeast- and northwest-directed paleocurrents for the Shizigou Fm. strata.

4.2. Framework grain compositions

Sandstone samples from the HT section are poorly-moderately sorted with majority of subangular-subrounded and minority of angular-subangular grains (Fig. 3G–I). The framework grains include predominant quartz (38.22%–66.47%) and lithic fragments (21.69%–47.91%) and subordinate feldspar (8.64%–23.88%). Plagioclase takes more portions than K-feldspar. The feldspars in lower Shang Youshashan Fm. samples suffered comparatively stronger weathering than that in other formation samples. There are mainly metamorphic (13.23%–31.46%) and sedimentary (5.72%–27.92%) lithic fragments, with minor igneous rock detritus. The relative contents of these two types of lithic fragments are variable among the analyzed samples. Samples of Shang Youshashan Fm. contain substantially metamorphic lithic fragments (mainly quartzite, schist and phyllite), while samples of Shizigou Fm. and Qigequan Fm. show an increasing trend of sedimentary lithic fragments (mainly mudstone, chert, sandstone and carbonate). The abundances of quartz and lithic fragments shifted sharply during 14–12 Ma (Fig. 5A–C). The framework grain composition data plotted in the quartz-feldspar-lithics (Q-F-L) provenance discrimination ternary diagram indicate that the HT section sandstones were mainly supplied from recycled orogenic sources (Fig. 5D).

4.3. Heavy minerals

Transparent heavy minerals in the HT section samples are mainly composed of hornblende (39.34%–76.96%, avg. 56.38%) and garnet (6.15%–43.65%, avg. 21.61%), and minor epidote, zircon, tourmaline, chlorite and biotite (Fig. 3F). These heavy minerals overall indicate low compositional and textural maturity. Hornblende and zircon grains are dominantly angular and minorly subrounded in shape. The ZTR index (sum of the proportions of zircon, tourmaline and rutile in transparent

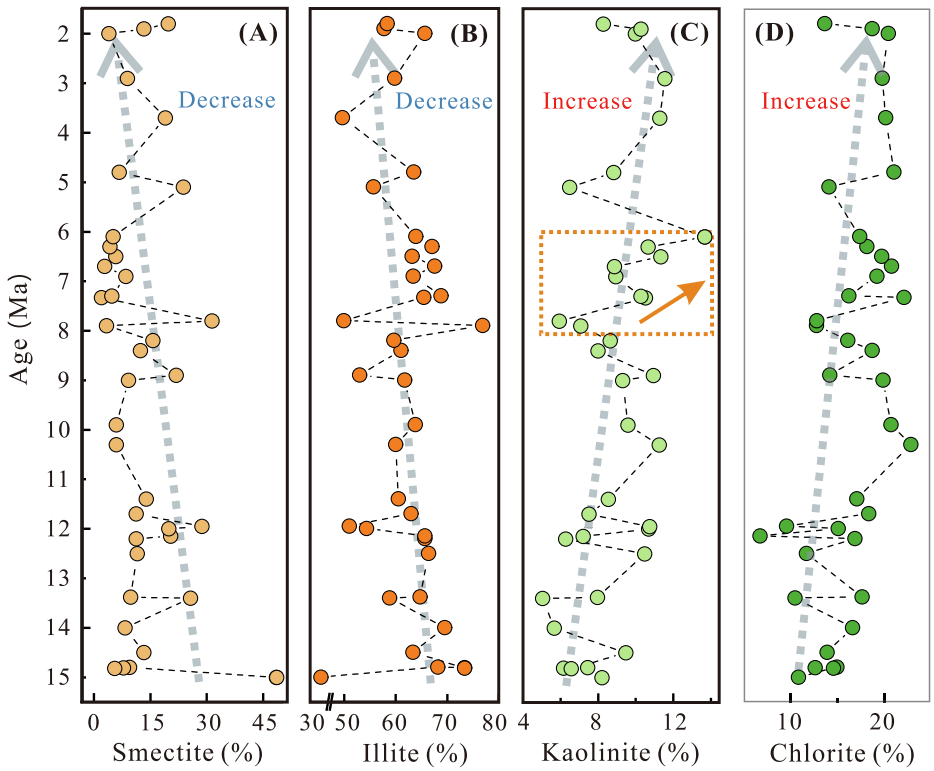

Fig. 6. Variations in the proportion of clay minerals since the middle Miocene (15.3–1.8 Ma), i.e., (A) smectite, (B) illite, (C) kaolinite, (D) chlorite. The general trends of kaolinite and illite contents over time in the Huaitoutala area are decoupled with climatic conditions, indicating the influence of source material supply. Yet, the increasing kaolinite content in 8–6 Ma samples corresponded to the enhanced precipitation.

heavy minerals), which is commonly used in evaluation of sediment maturity (Hubert, 1962; Andò et al., 2012; Garzanti et al., 2015), is relatively low (2–10) (Fig A. 1).

4.4. Bulk mineral compositions

The results of bulk XRD analysis show consistent mineralogical compositions of fine-grained sedimentary rocks in the HT section. The main mineral components include quartz (14.3%–38.9%, avg. 27.1%), plagioclase (5.95–32.6%, avg. 15.1%), K-feldspar (1.7%–14.6%, avg. 7.3%), calcite (2.2%–20.9%, avg. 9.8%) and clay minerals (16.4%–60.4%, avg. 40.4%). Values of the clay/Q ratio range from 0.46 to 4.78. For the related sample diffractograms and mineral characteristic peak information, refer to the appendix Fig A. 2.

4.5. Clay minerals

Clay mineral assemblages of the analyzed samples mainly consist of illite (abbr. Ill, 32.43%–76.84%, avg. 61.78%), chlorite (Chl, 6.76%–22.8%, avg. 16.37%), smectite (Sme, 1.97%–48.52%, avg. 12.95%) and kaolinite (Kln, 5.04%–13.68%, avg. 8.91%). The diffraction patterns of typical samples are shown in the appendix Fig A. 3. The distributions of clay minerals in Fig. 6 display increasing trends of chlorite and kaolinite contents and decreasing trends of smectite and illite contents with time (15.3–1.8 Ma). Illite chemistry index (CI) ranging from 0.25 to 0.50 (Fig A. 4F) reveals Fe-Mg rich illite and strong physical weathering. Illite crystallinity index (KI) ranging from 0.26 to 0.45 (Fig A. 4E) indicates well crystalline of illite and moderate chemical weathering. Values of widely used clay mineral ratios, including Kln/Chl, Kln/Ill, Kln/Sme and (Kln + Sme)/(Ill + Chl), were calculated and presented in appendix Fig A. 4A–D. Values of Kln/Chl and (Kln + Sme)/(Ill + Chl) ratios keep stable, while values of Kln/Ill and Kln/Sme ratios increased slightly over time. Although the changing trends of clay mineral ratios are inconsistent, the notable shifts of values occurred at 12 Ma, 9 Ma and 8–7 Ma.

4.6. Major and trace element compositions

Major elemental ratios (i.e., Na/Al, Na/K, K/Al, Ca/Ti, Ca/Al and Ca/K) were calculated based on the geochemical results of 33 analyzed samples (Fig A. 5). The values of Na/Al, Na/K ratios are relatively stable for 15.3–12 Ma samples (avg. 0.10 and 0.33, respectively) and indicate slightly increasing trends for 12–1.8 Ma samples (avg. 0.12 and 0.40), and are highly variable for 9–6 Ma samples. The K/Al ratio (avg. 0.31 in 15.3–1.8 Ma) is negatively correlated with Na/Al, Na/K ratios and shows an overall increasing trend. The Ca/Ti, Ca/Al and Ca/K ratios are at stable low values (avg. 1.31, 0.07 and 0.23 in 15.3–1.8 Ma, respectively), except for the obvious increase in 12–9 Ma. The element compositions of sediment samples normalized to the Upper Continental Crust (UCC) composition (Taylor and McLennan, 1985) are shown in Fig A. 6C, which exhibiting similar Na-, Ca-, Sr-depleted, K-stable and Al-enriched phenomena in sediments compared to UCC.

Due to the inherited characteristics of REE to source materials, the distribution pattern of REE in sediments is often used to indicate geochemical features of parent rocks (McLennan, 1989; Cao et al., 2015; Fathy et al., 2018). It can be seen from Fig A. 6A that the distribution patterns of chondrite-normalized (Sun and McDonough, 1989) REE in the HT samples are consistent and basically similar with that of the UCC and Post-Archean Australian Shale (PAAS) (Taylor and McLennan, 1985), distinguished by LREE enrichment (light REE, i.e., La–Eu), HREE depletion (heavy REE, i.e., Gd–Lu), negative Eu anomaly (La_N/Yb_N = 11.03–12.61, Gd_N/Yb_N = 1.56–1.80, Eu/Eu*=0.60–0.64). Samples of the three formations plotted on the La-Th-Sc ternary diagrams are located on similar positions which near the La apex and further away from the Sc apex (Fig A. 6B).

5. Discussion

5.1. Provenance of the late Cenozoic sedimentary rocks in the northeastern Qaidam Basin

The difference of source rock lithology may significantly affect chemical weathering process and also influence the application and interpretation of chemical weathering proxies. Thus, sedimentary sources and parent-rock lithology should be investigated prior to chemical weathering intensity reconstruction. The information achieved by chondrite-normalized REE patterns, La-Th-Sc ternary plots and Q-F-L ternary plots suggest that the analyzed HT sedimentary strata were mainly derived from intermediate-felsic type parent-rocks within recycled orogenic sources (Fig A. 6). Moreover, the low textural and compositional maturity of sandstones imply short-distance sediment transport and proximal accumulation, which is evidenced by the angular-subangular grains, moderate-poor sorting, high proportion of unstable minerals (e.g., hornblende) and low ZTR values (2–10). The abundant metamorphic and metasedimentary lithic fragments (13.23%–31.46%, avg. 20.62%) in the sandstone compositions match well to the Precambrian metamorphic basement and the exposures of the early Paleozoic UHP metamorphic rocks in the South Qilian-North Qaidam belt. Heavy mineral assemblages of the analyzed samples in this study are mainly composed of hornblende, garnet and epidote. The published mineralogical data of the NE Qaidam Basin include epidote and garnet-dominate heavy mineral assemblages and Fe-, Mn-rich detrital garnets in the Cenozoic sedimentary rocks (Jian et al., 2013a; Hong et al., 2020; Nie et al., 2020), further suggesting predominant derivation of metamorphic, metasedimentary and magmatic rocks.

The published detrital zircon U-Pb age patterns of the Cenozoic sedimentary rocks from the Huaitoutala and Dahonggou sections are commonly distributed in three major age populations, including Proterozoic (2.5–1.6 Ga), early Paleozoic (500–400 Ma) and Permian-Triassic (300–200 Ma) (Bush et al., 2016; Zhuang et al., 2019; Yin et al., 2020). The Paleoproterozoic and late Cambrian-early Devonian zircon age populations are corresponding to the metamorphic crystalline basement and magmatic rocks in the South Qilian Shan, respectively (Cowgill et al., 2003; Gehrels et al., 2003; Yan et al., 2010; Menold et al., 2016). Recently published researches attribute the Permian-Triassic (300–200 Ma) zircon age populations to recycling of the Cenozoic-Mesozoic sedimentary strata (clastic materials supplied from the Eastern Kunlun Shan) (Mo et al., 2007; Wu et al., 2011; Yu et al., 2017; Jian et al., 2018; Peng et al., 2018; Lu et al., 2019; Song et al., 2019) and the isolated Permian-Triassic granite plutons (Chen et al., 2012; Cheng et al., 2017; Jian et al., 2020b; Zhang et al., 2021a) in the North Qaidam metamorphic belt and Qilian Shan-Nan Shan regions. Results of detrital apatite fission-track (AFT) ages distribution in the Honggou section (Wang et al., 2017b), Zongwulong Shan and Huaitoutala section (Pang et al., 2019) show significant changes of the population peak ages at ca. 12 Ma, 18–11 Ma, 7 ± 2 Ma, respectively, indicating rapid exhumation and deformation of South Qilian-North Qaidam ranges. Conglomerate clast composition for the HT section dominated by carbonate, granite, intraformational limestone, which match rock units in the northern Qaidam Basin ranges (e.g., the Olongbuluke and Zongwulong mountains) (Zhuang et al., 2011a). Additionally, the main SW-oriented paleocurrents in this study (Fig. 4) and previously published paleocurrent data (Zhuang et al., 2011a; Bush et al., 2016; Pang et al., 2019) further confirm sediment sources to the northeast of the Huaitoutala location.

Combining the comprehensive multi-proxy evidences in this study and previous studies, it is concluded that the source of the late Cenozoic Huaitoutala sedimentary strata (15.3–1.8 Ma) was almost unchanged and constrained within the South Qilian Shan and the North Qaidam belt. The parent rock types in the source area are dominated by felsic igneous and metamorphic rocks and compositionally felsic-equivalent rocks.

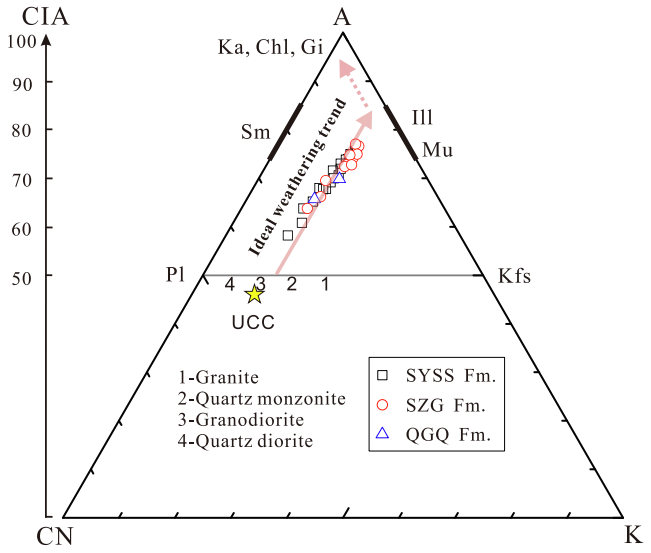

Fig. 7. A-CN-K (Al_2O_3-CaO + Na_2O-K_2O) plot of the analyzed Huaitoutala samples from the Shang Youshashan (SYSS), Shizigou (SZG) and Qigequan (QGQ) formations. The pink lines with arrows show predicted weathering trends, modified from Jian et al. (2019). Samples are on the ideal trend line, indicating negligible influence of the diagenetic K metamorphism on chemical weathering evaluation. The initial compositions of source rocks are similar to quartz monzonite and granodiorite. Ka: Kaolinite, Chl: Chlorite, Gi: Gibbsite, Sm: Smectite, Ill: Illite, Mu: muscovite, Pl: Plagioclase, Kfs: K-feldspar, UCC: Upper Continental Crust. (For interpretation of the references to colour in this figure legend, the reader is referred to the web version of this article.)

5.2. Chemical weathering intensity history since 15.3 Ma

Various geochemical proxies have been proposed to quantitatively evaluate the intensity of silicate chemical weathering based on differences in elemental mobility (e.g., Shao et al., 2012; Roy and Roser, 2013; Clift et al., 2014; Zhao and Zheng, 2015; Perri, 2018; Cao et al., 2019; Ren et al., 2020). It is well known that the chemically-active alkali and alkaline earth metals (e.g., K, Na, Ca, Mg, Sr) are prone to be depleted and migrate as dissolved ions during chemical weathering processes, while the stable elements like Al and Ti tend to preserve in solid residues (Nesbitt and Young, 1982; Duzgoren-Aydin et al., 2002; Chen et al., 2020). Here, we selected a few representative indicators, from double-element ratios (i.e., Na/Al and SiO_2/Al_2O_3) to multiple-element ratios (i.e., CIA, CIW, PIA, α^{Al}Na and ICV, formulas are detailed in Fig A. 8), to reconstruct the history of paleo-chemical weathering intensity. Chemical Index of Alteration (CIA) and the A-CN-K (Al_2O_3-CaO + Na_2O-K_2O) diagram (Nesbitt and Young, 1982, 1984) are quantitatively used to trace chemical weathering processes and even to constrain initial compositions of source rocks. Chemical Index of Weathering (CIW, Harnois, 1988) and Plagioclase Index of Alteration (PIA, Fedo et al., 1995) were modified on the basis of CIA to eliminate the influence of potassium mobility on chemical weathering proxies. Note that CaO* in calculation formulas refers to CaO incorporated in silicate minerals (McLennan, 1993; Li and Yang, 2010). α^{Al}Na reflects chemical weathering degrees by comparing the differences of element concentrations in target samples and in UCC (Garzanti et al., 2013b). The compositional maturity of fine-grain sediments represented by Index of Compositional Variability (ICV) can also indicate chemical weathering intensity (Cox et al., 1995; Cullers and Podkovyrov, 2000).

The Q/(Q + F) ratio and clay mineral assemblage were also employed as chemical weathering proxies (Rieu et al., 2007; Kamp, 2010; Garzanti et al., 2013a; Mei et al., 2021). Clay minerals, as typical weathering products, were thought to be faithful indicators of climatic and regional chemical weathering evolutions. Generally, kaolinite is formed by strong leaching, hydrolysis and chemical weathering

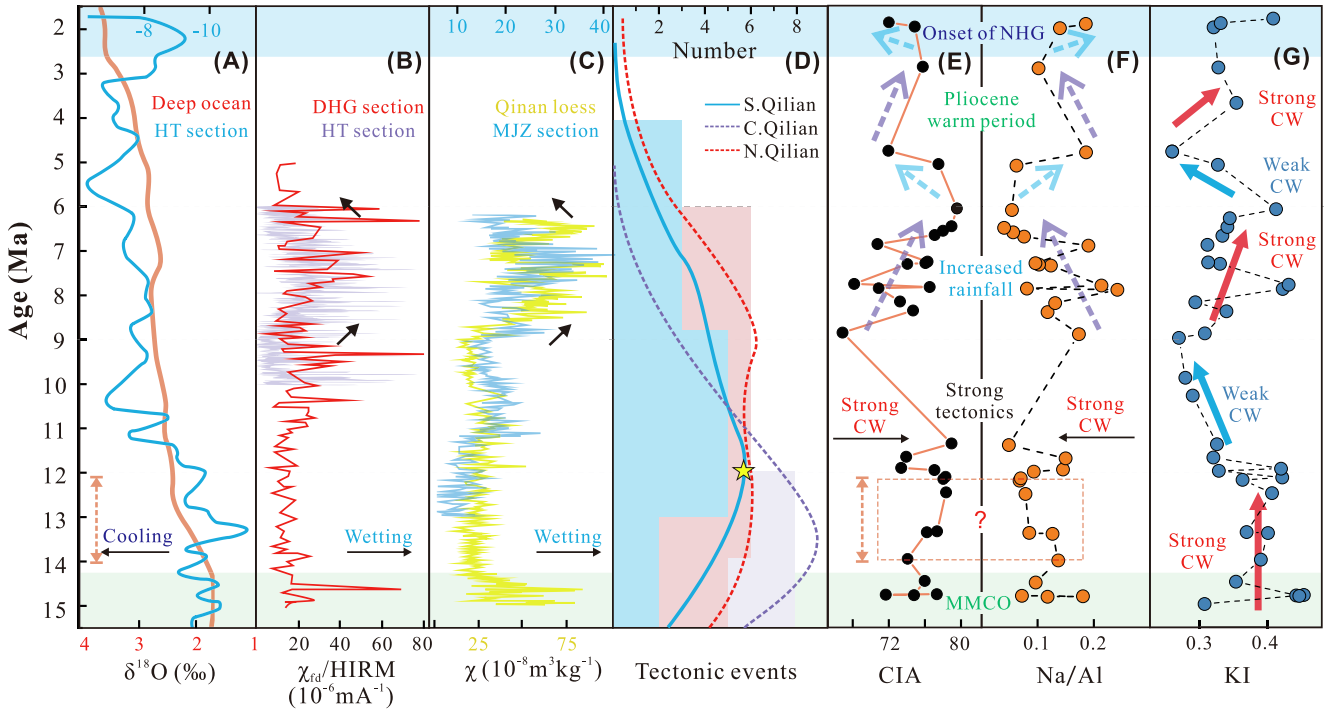

Fig. 8. Comparison of chemical weathering records (15.3–1.8 Ma) revealed by CIA, Na/Al and illite crystallinity index (KI) proxies (E–G, this study), as well as climatic (A–C) and tectonic (D) evolution records from published studies. (A) The oxygen isotope records ($\delta^{18}O$) of global deep-sea (Zachos et al. (2001); in red) and the Huaitoutala section (Zhuang et al. (2011b); in blue). (B) The χfd/hard isothermal remanent magnetization (HIRM) records from the Huaitoutala (HT, in purple) and Dahonggou (DHG, in red) sections in the Qaidam Basin, after Nie et al. (2017, 2020). (C) The magnetic susceptibility records of Qinan loess-soil sequence in the Loess Plateau from Guo et al. (2002) and Mojiazhuan (MJZ) section in the Xining basin from Zan et al. (2018). (D) Probability temporal distribution histogram of the late Cenozoic tectonic events recorded in the South Qilian Shan (blue), Central Qilian Shan (purple) and North Qilian Shan (red) modified after Li et al. (2020), as constrained by published thermochronological, sedimentological and other methods data. Note that the other geochemical indices of chemical weathering not shown here demonstrate a consistent chemical weathering trend with CIA (Fig A. 8). The increase of precipitation-sensitive proxy (χfd/HIRM and χ) in 9–6 Ma (B–C) suggested the intensified precipitation in the Qaidam Basin and surrounding regions. Statistic results show that the South Qilian Shan was tectonically active in 12–9 Ma, with the most impactful event at ca. 12 Ma (represented by the yellow asterisk). CIA = $Al_2O_3/(Al_2O_3 + K_2O + CaO^* + Na_2O) \times 100$. (For interpretation of the references to colour in this figure legend, the reader is referred to the web version of this article.)

(Chamley, 1989; Scarciglia et al., 2005; Dypvik et al., 2011; Wang et al., 2020b). Illite and chlorite are usually produced under poor hydroclimatic conditions and rapid physical erosion (Selvaraj and Chen, 2006; Liu et al., 2007b, 2012). Smectite is derived from environments with seasonal dry-wet fluctuation, moderate chemical weathering and poor drainage (Godet et al., 2008; Liu et al., 2009; Xu et al., 2012; Song et al., 2018a). Furthermore, the crystalline characteristics of illite reflected by CI and KI proxies can express the intensity of chemical and physical weathering (Esquevin, 1969; Gingele et al., 1998; Liu et al., 2008; Alizai et al., 2012).

In order to better reconstruct chemical weathering evolution, it is necessary to eliminate the interferences in sedimentary source-to-sink process, i.e., (1) source rock composition, (2) hydrodynamic sorting (Garzanti et al., 2011; Jian et al., 2013b), and (3) K metamorphism and smectite-illite conversion during diagenesis. Our new data suggest the Huaitoutala sedimentary strata are derived from felsic metamorphic and igneous rocks with consistent geochemical composition. The source rock is similar to quartz monzonite and granodiorite as shown in the A-CN-K diagram (Fig. 7). We have chosen fine-grained samples (paleosols and mudstones) for geochemical and clay mineralogical determination to minimize the disturbance of hydraulic-sorting on mineral and chemical compositions. Our results in Fig A. 7 show that there are no obvious correlations between the CIA values, (Sme + Kln)/(Ill + Chl) ratios and the clay/quartz ratios (clay/quartz is highly dependent on sediment grain sizes, i.e., the hydrodynamic sorting), indicating that hydrodynamic sorting might have little influence to these chemical weathering proxies. Major elemental data plotted on the A-CN-K diagram present an ideal weathering trend, proving nonexistence of diagenetic K-metasomatism (kaolinite converts to illite) (Fedo et al., 1995; Cullers and Podkovyrov, 2000). Smectite is prone to transform into illite during diagenesis under the conditions of burial depth > 1500 m, pressure of 900–920 kg/cm^2 and temperature of 100–140 °C (Song et al., 2018b). Although 4570 m-thick sedimentary strata (Fang et al., 2007) makes the HT section a qualified environment for transformation, the smectite contents do not decrease with burial depth as expected (Fig. 6A). Therefore, we conclude that these chemical weathering proxies are independent of above factors.

The temporal variations of geochemical proxy value for the analyzed samples are shown graphically in Fig A. 8. The CIA values vary between 66.86 and 79.54 with a mean of 75.10 during 15.3–1.8 Ma period. The CIW and PIA values are in the range of 76.79–93.78 (avg. 88.27) and 72.74–92.34 (avg. 85.85), respectively. The values of $\alpha^{Al}Na$, ICV, Na/Al and SiO_2/Al_2O_3 ratios separately vary within 1.49–8.98 (avg. 3.78), 0.78–1.23 (avg. 0.96), 0.04–0.24 (avg. 0.12) and 2.71–5.79 (avg. 3.82). According to these results, the northern Qaidam Basin has experienced moderate chemical weathering since the middle Miocene. It is further confirmed by the data plotted in the A-CN-K diagram (Fig. 7) and the evolution trends of Na/Al, Na/K, K/Al and Ca/Al ratios (Fig A. 5). Anorthite (Ca-rich) is preferentially weathered than albite (Na-rich), and finally K-feldspar (K-rich), resulting in the sequential loss of Ca, Na and K during chemical weathering (Nesbitt et al., 1996). Thus, the depleted Ca, Na and stable K contents illustrate that chemical weathering was in plagioclase-weathering stage with moderate intensity.

The geochemical proxies and the KI values show consistent evolution trends of chemical weathering intensity over time. Chemical weathering was relatively strong in 15.3–12 Ma, weakened in 12–9 Ma, enhanced in

9–6 Ma and slightly weakened after 6 Ma (Fig A. 8; Fig. 8). Collectively, we suggest an overall moderate chemical weathering intensity in the northern Qaidam Basin since the middle Miocene. The regional development of chemical weathering can be further divided into four stages, including phased intensification in 15.3–12 Ma and 9–6 Ma, and phased repression in 12–9 Ma and < 6 Ma.

5.3. Controlling factors of chemical weathering process in the NE Tibetan Plateau

The late Cenozoic climatic and tectonic changes have long been considered as the principal driving forces of chemical weathering evolution in the northeastern Tibetan Plateau (e.g., Bao et al., 2019; Fang et al., 2019; Ren et al., 2019). Furthermore, the global cooling-controlled long-term reduction of chemical weathering intensity across the NE Tibetan Plateau was also suggested by previous studies (e.g., Bao et al., 2019; Liu et al., 2020), however, is not reflected by the results in this study. Our geochemical and mineralogical records (Fig. 8E–G, Fig A. 8) demonstrate an inspiriting positive shift of chemical weathering intensity in 9–6 Ma interval. The phased chemical weathering changes (15.3–12 Ma, 12–9 Ma, 9–6 Ma, <6 Ma) can be attributed to diverse influencing factors of both climate change and tectonics.

5.3.1. 15.3–12 Ma

Our results indicate relatively high chemical weathering intensity in the 15.3–12 Ma interval (Fig. 8E–G). The intense chemical weathering in the early stage (15.3–14 Ma) corresponded well to high precipitation and temperature in the MMCO (18–14 Ma) (Miao et al., 2013). After that, the Earth's climate has experienced a rapid cooling during 14–12 Ma with significant increase of the deep-sea $\delta^{18}O$ value (Fig. 8A) and sharp drop of the sea surface temperature (Zachos et al., 2001, 2008; Shevenell et al., 2004; Ma and Jiang, 2015). However, the intensity of chemical weathering documented in the HT section has not reduced in the context of global cooling. The decoupling of global cooling and chemical weathering may imply an overwhelming effect of local climate on chemical weathering in the Qaidam Basin, rather than global climate. We assume that the local climate is not completely controlled by the global climate, and hence the NE Tibetan Plateau could keep wet and warm climate for maintaining the strong chemical weathering in 14–12 Ma. Perhaps the tectonic and topographic factors played a vital role in this event. The specific reason remains to be fully explored and understood.

5.3.2. 12–9 Ma

We suggested that the dramatic decrease of chemical weathering intensity in 12–9 Ma is intimately associated with rapid tectonic uplift and exhumation of the Qilian Shan. The Qilian Shan thrust belt was tectonically active since ~ 16 Ma and reached a peak at 13–12 Ma (Fig. 8D, Li et al., 2020). Published thermochronological, magnetostratigraphic and sedimentological data suggest a prominent tectonic uplift in the South Qilian Shan and topographic growth southward to the northern margin of the Qaidam Basin occurred at ~ 12 Ma (Lu and Xiong, 2009; He et al., 2018; Meng et al., 2020). Surface uplift amplitude of the northern Tibetan Plateau since the middle Miocene is inferred to be approximately 1700 m with the initial elevation of 2700 m (Li et al., 2011). The paleo-altimetry studies based on carbon and oxygen isotope analysis show that the average altitude of Qilian range in the early Miocene was 2848 m, and after intensive exhumation, it was uplifted to 3586 m in the middle Miocene (Qi et al., 2015). In addition, the adjacent Qaidam Basin has raised by ca. 250 m (2100 m–2350 m) during 12–9 Ma period for sedimentary accumulation and crustal shortening (Li et al., 2017; Yu et al., 2021). Based on these backgrounds, we favor that the intensive exhumation and denudation of the South Qilian Shan at 12–9 Ma induced strong and rapid physical erosion, resulting in oversaturation of fresh material supply and reduction of sediment residence time. And the chemical weathering regime in this period might to be kinetic-limited, rather than supply-limited. Previous studies suggest that kinetic-limited weathering processes are quite common in tectonically-active orogenic regions (Riebe et al., 2004, 2017; West et al., 2005; Sun et al., 2019). Under kinetic-limited weathering conditions, chemical weathering rates no longer increase proportionally with the supply rates of fresh minerals, but are tightly coupled to the kinetic dissolution rates of minerals (Ferrier et al., 2016). It is unconducive to facilitate chemical weathering because the limitation has transformed from supply of fresh material to climatic factors (i.e., temperature and precipitation) (Gabet and Mudd, 2009; Dixon et al., 2012).

In addition, water limitation in the Qaidam Basin further decouples the positive correlation between chemical weathering and physical erosion, thereby promoting the transition of weathering regime to kinetic-limited (Rasmussen et al., 2011). The tectonics-driven intensified aridity (Cheng et al., 2019; Zhang et al., 2021b) has been revealed by the ~ 2.5‰ positive shift in the $\delta^{18}O$ values (Fig. 8A) from pedogenic and lacustrine carbonates in the Qaidam Basin (Zhuang et al., 2011b; Li et al., 2016), synchronous in the Tarim (Kent-Corson et al., 2009), Linxia (Dettman et al., 2003) and Xunhua basins (Hough et al., 2011). The regional aridity probably resulted from the retreat of the Paratethys (Ritts et al., 2008; Zhang et al., 2007), blockage of moisture from the Indian and Pacific oceans by the elevated Himalaya (Spicer et al., 2003), and blockage of westerlies air mass and moisture from the Atlantic and Arctic oceans by uplift of basin-bounding mountains in the northern Tibetan Plateau (Altyn Shan, Qilian Shan, Tian Shan and Pamir) (Zhuang et al., 2011b; Liu et al., 2015; Hou et al., 2021).

5.3.3. 9–6 Ma

Although the traditional opinion suggests that chemical weathering in the NE Tibetan Plateau was persistently weakened since the MMCO (Yang et al., 2016; Bao et al., 2019), our results reveal increased chemical weathering intensity in the Qaidam Basin during 9–6 Ma (Fig. 8E–G). As several studies suggest relatively high precipitation around the HT section regions and in the South Qilian Shan (Nie et al., 2017, 2020), we believe that the intensification of chemical weathering is a response to increasing humidity during this period, rather than changes in temperature and tectonic activities. Recently, many studies emphasized the importance of humidity to chemical weathering evolution, instead of temperature (Graly et al., 2014; Scribner et al., 2015; Calabrese and Porporato, 2020). The magnetic susceptibility χ and χfd/HIRM records, which are sensitive to rainfall variation, exhibited relatively high precipitation values during the 9–6 Ma period (Fig. 8B–C). Recent calculation results demonstrate that the mean summer precipitation around the HT section area during 8.25–7.45 Ma (62 mm) is twice of the current level (ca. 32 mm) (Gao et al., 2021). Regionally, the significant increase in precipitation is also observed simultaneously at the Mojiazhuan (MJZ) section in the Xining basin (Zan et al., 2018), Qinan loess-soil sequence in the Loess Plateau (Guo et al., 2002), and Wushan (WS) section in the Wushan basin (Wang et al., 2021). The mineralogical proxies of red clay sequence from the western Loess Plateau, including large fluctuations of calcite content, low protodolomite content, increasing illite and decreasing chlorite contents, indicate that the climate was relatively humid with seasonal wet-dry fluctuations in the late Miocene (9.5–5 Ma) (Sun et al., 2015). Additionally, the fossil wood data also suggested that the climate was moist enough to support forest ecosystem in the northern Qaidam Basin during the late Miocene (Cheng and Yang, 2016; Ren et al., 2020).

Although all the evidences reveal intensified humidity in the northeastern Tibet and in the surrounding regions during 9–6 Ma, formation mechanism of the wetting period in the HT section still remains an open question. There are at least two possibilities. 1) The increased humidity was a regional climatic event and was probably attributed to the strengthened East Asian summer monsoon by uplift-driven high topography of the northern and eastern Tibet through intensification of the thermal contrast and pressure gradient between land and ocean. This hypothesis is supported by magnetic and paleontological evidences and

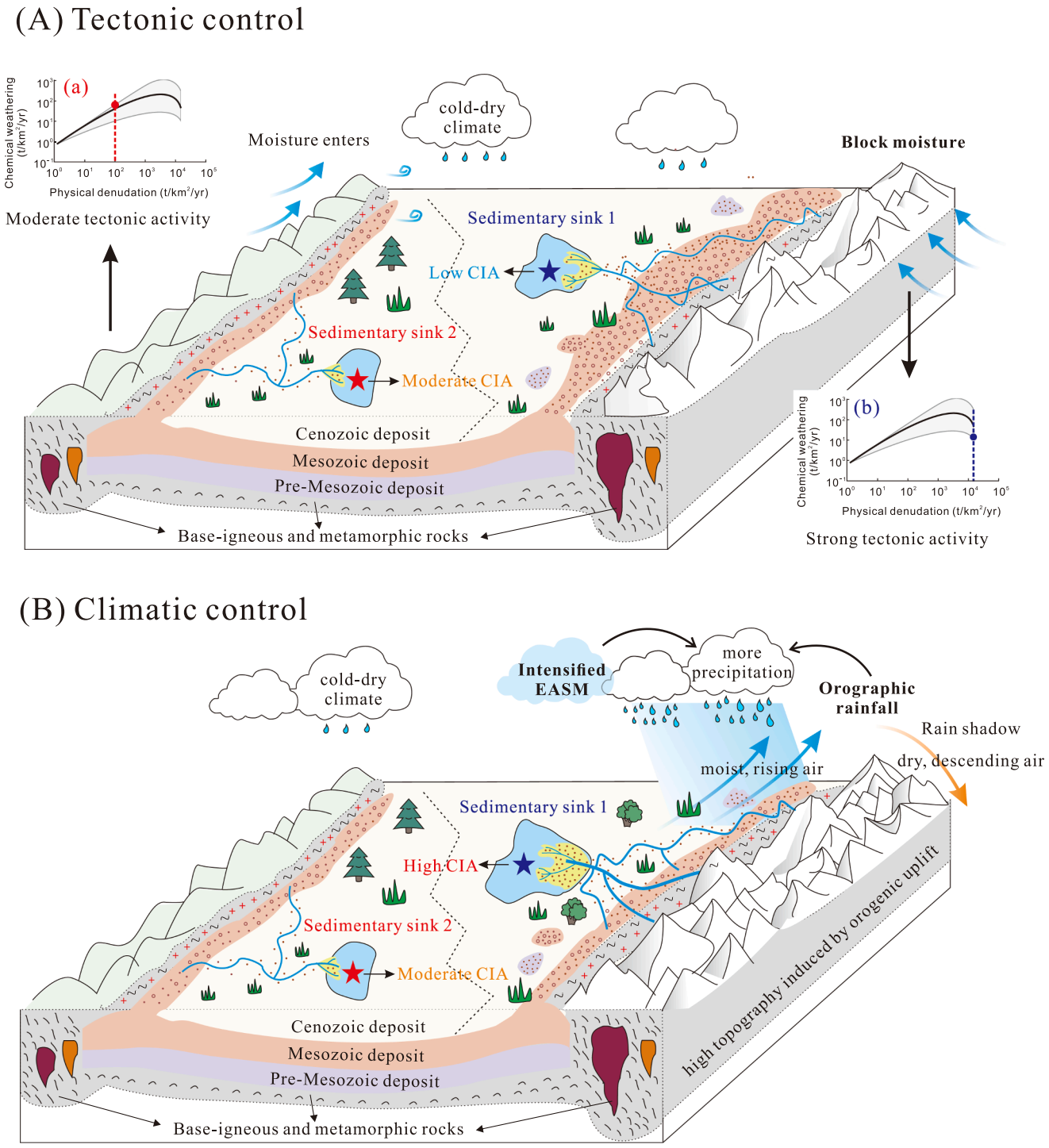

Fig. 9. Conceptual models showing the evolutionary mechanism of the late Cenozoic chemical weathering in the NE Tibetan Plateau controlled by (A) tectonics (12–9 Ma) and (B) climate (9–6 Ma). Two sediment sinks are arranged in each picture. The sedimentary sink 2 (red star) is set as the control group with moderate chemical weathering intensity, and the sedimentary 1 (blue star) is set to respond to tectonic or climatic changes. Igneous (red cross) and metamorphic (black tilde) basements are drawn on grey background. In tectonic-control period (A), strong tectonic uplift and deformation of mountains (right) reduce chemical weathering intensity in sedimentary sink 1 by enhanced physical denudation and shortened residence time. The chemical weathering regime change from supply-limited (a, sink 2) to kinetic-limited (b, sink 1) for the excessive physical erosion rate, and thus inhibiting chemical weathering in sink 1. The moisture is blocked by the growing mountains, resulting in the enhancement of aridity and further reduction of chemical weathering. Note that, the supply-limited (a) and kinetic-limited (b) figures are modified after Gabet and Mudd (2009). In the climate-control period (B), the regional chemical weathering is intensified by the increased precipitation in the sink 1. There exist two possibilities for the increase of regional precipitation, i.e., (1) the intensified East Asian summer monsoon or (2) the orographic rainfall on the windward slopes by high elevation. (For interpretation of the references to colour in this figure legend, the reader is referred to the web version of this article.)

by numerical modeling results (An et al., 2001; Nie et al., 2017; Ren et al., 2020; Zhao et al., 2020; Hui et al., 2021; Wang et al., 2021). Moreover, the expansion of evergreen broadleaf forests in southeastern Asia during the Miocene recorded in floral fossils indicate a possibility of increased winter precipitation due to weakening of the Asian winter monsoon (Li et al., 2021). 2) The increased humidity was a local event that happened in the northern Qaidam Basin. In this case, orographic rainfall is a reasonable explanation for local humidification in the context of intensified regional aridity (Miao et al., 2012; Nie et al., 2020). The dynamics of orographic precipitation in an alpine terrain show forced ascending of air and increased rainfall on the windward slopes, and conversely, formation of the rain shadow and decreased rainfall on the leeside (Roe et al., 2003; Liu et al., 2015; Geng et al., 2017). The high topography of the South Qilian Shan in the late Miocene forced the northward air mass to climb, resulting in the humidification in the northern part of the Qaidam Basin.

5.3.4. 6 Ma to present

The variations of chemical weathering intensity since 6 Ma include a rapid decrease at ~ 5 Ma, steady increase in 5–3 Ma and decrease < 3 Ma. The northwestward shift of EASM during the Pliocene warm period provided a warm climate and enhanced precipitation in the NE Qaidam Basin (Mutz et al., 2018; Huang et al., 2019; Ren et al., 2020), which is evidenced by the occurrence of Ostracod faunas in the Qinghai Lake sediments during 4.6–3.6 Ma period (Lu et al., 2017). The warm and wet climate may promote the development of chemical weathering in the Qaidam Basin in 5–3 Ma. Published models show that the expansion of Arctic ice-sheet (<3 Ma) strengthened the East Asian winter monsoon and induced southward shift of the westerlies by intensifying the Siberian High, and thus enhanced aridification in the NE Tibetan Plateau (Ge et al., 2013; Lu et al., 2020). In this case, the onset (ca. 3.6 Ma) and intensification (ca. 2.6 Ma) of Northern Hemisphere Glaciation (NHG) probably exercised a primary control over the weakened chemical weathering (<3 Ma) of the Qaidam Basin (Lu et al., 2020; Koutsodendris et al., 2019). The analyzed samples in < 6 Ma interval are insufficient to do analysis with high temporal resolution. Therefore, the history of chemical weathering intensity and controlling factors from 6 Ma to present remain uncertain and require further investigation.

In summary, the history of chemical weathering intensity in the northern Qaidam Basin during the late Cenozoic can be divided into four stages with distinctive controlling factors: (1) In 15.3–12 Ma, regional climate took a main control of chemical weathering. (2) In 12–9 Ma, as shown in the conceptual model (Fig. 9A), the strong orogenic uplift significantly restricted chemical weathering by reinforcement of physical denudation, regional aridification and reduction of fresh mineral residue time. (3) In 9–6 Ma, the complex tectonics-climate interactions (Fig. 9B), namely, orographic rainfall and/or intensified East Asian monsoon precipitation by high elevation, resulted in humid climate and enhanced chemical weathering. (4) 6 Ma to present, the evolution of regional chemical weathering was synchronous with global climate change including the expansion of EASM during the Pliocene warm period and the onset of NHG in the Quaternary.

5.4. Implications

The paleo-chemical weathering intensity is commonly used to reconstruct regional paleoclimatic and paleoenvironmental history (Kump et al., 2000; Zhai et al., 2018; Cao et al., 2019; Wang et al., 2020a). We argue that the fluctuations of chemical weathering intensity from sedimentary records should not be simply attributed to climatic factors, especially in those regions with high erosion rates. Tectonic uplift and deformation can significantly vary physical denudation rates and patterns, local topography, clastic material supply pathways and rates and sedimentary environments (Zhang et al., 2017; Zhu et al., 2017), and thus result in variations in chemical weathering intensity.

The petrological and mineralogical proxies, i.e., the ratios of framework grains (Q/(Q + F)) and clay mineral contents in sediments, exhibit low sensitivity to chemical weathering evolution in the study area. For example, the Q/(Q + F) values remain stable only with a few rapid shifts at 13–12 Ma and ~ 7 Ma (Fig A. 4G). The values of smectite, illite, kaolinite and chlorite contents (Fig. 6) and clay mineral ratios (e.g., Kln/Ill, Kln/Sme, Fig A. 4) are decoupled with chemical weathering in most analyzed samples, except for samples in 9–6 Ma and ~ 15 Ma intervals which were under the control of relatively warm and wet climatic conditions. This study shows that geochemical proxies (e.g., CIA, CIW, PIA, $\alpha^{Al}Na$; Fig A. 8) and illite crystallinity index (KI) are robust indicators for chemical weathering intensity. Note that, a comprehensive use of multiple methods is necessary to evaluate the influences from provenance changes, hydraulic sorting and even burial diagenesis in order to effectively reconstruct paleo-chemical weathering and to distinguish controlling factors.

6. Conclusions

This study conducted petrography, heavy mineral analysis, clay mineralogy, and element geochemistry on the Cenozoic sedimentary strata from the Huaitoutala section of the Qaidam Basin to reconstruct chemical weathering history and its driving forces in the northeastern Tibetan Plateau. We yield the following conclusions:

(1) The northern Qaidam Basin sediments were sourced from the South Qilian Shan and the North Qaidam belt and experienced an overall moderate chemical weathering since the middle Miocene, showing a high chemical weathering intensity in 15.3–12 Ma and continuous evolution of weakened-intensified-weakened weathering intensity in the 12–9 Ma, 9–6 Ma, and < 6 Ma periods, respectively.

(2) The late Cenozoic chemical weathering intensity in the northeastern Tibetan Plateau was controlled both by climatic and tectonic factors. Local and global climate were the principal driving forces for the development of chemical weathering intensity in 15.3–12 Ma and < 6 Ma, respectively. Strong tectonic activity in the NE Tibetan Plateau, especially rapid uplift and southward expansion of South Qilian Shan, significantly reduced the intensity of chemical weathering in 12–9 Ma by intensifying physical erosion and regional aridity. The enhanced chemical weathering in 9–6 Ma was tightly associated with the increasing precipitation induced by orographic rainfall and/or intensification of the East Asian summer monsoon. Our study emphasizes the importance of the tectonics-climate interactions for the evolution of regional chemical weathering degrees.

Declaration of Competing Interest

The authors declare that they have no known competing financial interests or personal relationships that could have appeared to influence the work reported in this paper.

Acknowledgments

This research was supported by the National Natural Science Foundation of China (No. 41902126) and Xiamen University Fundamental Research Funds for the Central Universities (No. 20720160114). We are grateful to editor Fabio Scarciglia and two anonymous reviewers for thoughtful and constructive comments on this manuscript.

Appendix A. Supplementary material

Supplementary data to this article can be found online at https://doi.org/10.1016/j.catena.2021.105785.

References

Alizai, A., Hillier, S., Clift, P.D., Giosan, L., Hurst, A., VanLaningham, S., Macklin, M., 2012. Clay mineral variations in Holocene terrestrial sediments from the Indus Basin. Quat. Res. 77 (3), 368–381. https://doi.org/10.1016/j.yqres.2012.01.008.

An, Z., Colman, S.M., Zhou, W., Li, X., Brown, E.T., Jull, A.T., Cai, Y., Huang, Y., Lu, X., Chang, H., Song, Y., Sun, Y., Xu, H., Liu, W., Jin, Z., Liu, X., Cheng, P., Liu, Y., Ai, L., Li, X., Liu, X., Yan, L., Shi, Z., Wang, X., Wu, F., Qiang, X., Dong, J., Lu, F., Xu, X., 2012. Interplay between the Westerlies and Asian monsoon recorded in Lake Qinghai sediments since 32 ka. Sci. Rep. 2 (1), 1–7. https://doi.org/10.1038/srep00619.

An, Z.S., Kutzbach, J.E., Prell, W.L., Porter, S.C., 2001. Evolution of Asian monsoons and phased uplift of the Himalaya-Tibetan plateau since Late Miocene times. Nature 411 (6833), 62–66. https://doi.org/10.1038/35075035.

An, Z.S., Wu, G.X., Li, J.P., Sun, Y.B., Liu, Y.M., Zhou, W.J., Cai, Y.J., Duan, A.M., Li, L., Mao, J.Y., Cheng, H., Shi, Z.G., Tan, L.C., Yan, H., Ao, H., Chang, H., Feng, J., 2015. Global monsoon dynamics and climate change. Ann. Rev. Earth Planet. Sci., 43, 29–77. DOI: 10.1146/annurev-earth-060313-054623.

Andò, S., Garzanti, E., Padoan, M., Limonta, M., 2012. Corrosion of heavy minerals during weathering and diagenesis: a catalog for optical analysis. Sed. Geol. 280, 165–178. https://doi.org/10.1016/j.sedgeo.2012.03.023.

Bao, J., Song, C., Yang, Y., Fang, X., Meng, Q., Feng, Y., He, P., 2019. Reduced chemical weathering intensity in the Qaidam Basin (NE Tibetan Plateau) during the Late Cenozoic. J. Asian Earth Sci. 170, 155–165. https://doi.org/10.1016/j.jseaes.2018.10.018.

Bao, J., Wang, Y., Song, C., Feng, Y., Hu, C., Zhong, S., Yang, J., 2017. Cenozoic sediment flux in the Qaidam Basin, northern Tibetan Plateau, and implications with regional tectonics and climate. Global Planet. Change 155, 56–69. https://doi.org/10.1016/j.gloplacha.2017.03.006.

Broccoli, A.J., Manabe, S., 1992. The effects of orography on midlatitude Northern Hemisphere dry climates. J. Clim. 5 (11), 1181–1201. https://doi.org/10.1175/1520-0442(1992)005<1181:TEOOOM>2.0.CO;2.

Bush, M.A., Saylor, J.E., Horton, B.K., Nie, J., 2016. Growth of the Qaidam Basin during Cenozoic exhumation in the northern Tibetan Plateau: Inferences from depositional patterns and multiproxy detrital provenance signatures. Lithosphere 8 (1), 58–82. https://doi.org/10.1130/L449.110.1130/2015362.

Calabrese, S., Porporato, A., 2020. Wetness controls on global chemical weathering. Environ. Res. Commun. 2 (8), 085005 https://doi.org/10.1088/2515-7620/abad7b.

Cao, L., Jiang, T., Wang, Z., Zhang, Y., Sun, H., 2015. Provenance of Upper Miocene sediments in the Yinggehai and Qiongdongnan basins, northwestern South China Sea: Evidence from REE, heavy minerals and zircon U-Pb ages. Mar. Geol. 361, 136–146. https://doi.org/10.1016/j.margeo.2015.01.007.

Cao, Y., Song, H., Algeo, T.J., Chu, D., Du, Y., Tian, L., Wang, Y., Tong, J., 2019. Intensified chemical weathering during the Permian-Triassic transition recorded in terrestrial and marine successions. Palaeogeogr. Palaeoclimatol. Palaeoecol. 519, 166–177. https://doi.org/10.1016/j.palaeo.2018.06.012.

Chamley, H., 1989. Clay Sedimentology. Springer, New York, p. 623.

Chen, Q., Li, Z., Dong, S., Yu, Q., Zhang, C., Yu, X., 2020. Applicability of chemical weathering indices of eolian sands from the deserts in northern China. Catena 198, 105032. https://doi.org/10.1016/j.catena.2020.105032.

Chen, X., Gehrels, G., Yin, A., Li, L., Jiang, R., 2012. Paleozoic and Mesozoic basement magmatisms of eastern Qaidam Basin, northern Qinghai-Tibet Plateau: LA-ICP-MS zircon U-Pb geochronology and its geological significance. Acta Geol. Sinica [English Edition] 86 (2), 350–369. https://doi.org/10.1111/j.1755-6724.2012.00665.x.

Cheng, F., Garzione, C.N., Mitra, G., Jolivet, M., Guo, Z., Lu, H., Li, X., Zhang, B.o., Zhang, C., Zhang, H., Wang, L., 2019. The interplay between climate and tectonics during the upward and outward growth of the Qilian Shan orogenic wedge, northern Tibetan Plateau. Earth Sci. Rev. 198, 102945. https://doi.org/10.1016/j.earscirev.2019.102945.

Cheng, F., Jolivet, M., Hallot, E., Zhang, D., Zhang, C., Guo, Z., 2017. Tectono-magmatic rejuvenation of the Qaidam craton, northern Tibet. Gondwana Res. 49, 248–263. https://doi.org/10.1016/j.gr.2017.06.004.

Cheng, Y.M., Yang, X.N., 2016. Miocene woods from the Qaidam Basin on northern Qinghai-Tibet Plateau with implications for paleoenvironmental change. J. Asian Earth Sci. 116, 198–207. https://doi.org/10.1016/j.jseaes.2015.11.022.

Clark, M.K., Farley, K.A., Zheng, D., Wang, Z., Duvall, A.R., 2010. Early Cenozoic faulting of the northern Tibetan Plateau margin from apatite (U–Th)/He ages. Earth Planet. Sci. Lett. 296 (1-2), 78–88. https://doi.org/10.1016/j.epsl.2010.04.051.

Clift, P.D., Hodges, K.V., Heslop, D., Hannigan, R., Van Long, H., Calves, G., 2008. Correlation of Himalayan exhumation rates and Asian monsoon intensity. Nat. Geosci. 1 (12), 875–880. https://doi.org/10.1038/ngeo351.

Clift, P.D., Wan, S., Blusztajn, J., 2014. Reconstructing chemical weathering, physical erosion and monsoon intensity since 25 Ma in the northern South China Sea: a review of competing proxies. Earth Sci. Rev. 130, 86–102. https://doi.org/10.1016/j.earscirev.2014.01.002.

Cowgill, E., An, Y., Harrison, T.M., Wang, X.F., 2003. Reconstruction of the Altyn Tagh fault based on U-Pb geochronology: Role of back thrusts, mantle sutures, and heterogeneous crustal strength in forming the Tibetan Plateau. J. Geophys. Res. 108 (B7), 2346. https://doi.org/10.1029/2002JB002080.

Cox, R., Lowe, D.R., Cullers, R.L., 1995. The influence of sediment recycling and basement composition on evolution of mudrock chemistry in the southwestern United States. Geochim. Cosmochim. Acta 59 (14), 2919–2940. https://doi.org/10.1016/0016-7037(95)00185-9.

Cullers, R.L., Podkovyrov, V.N., 2000. Geochemistry of the Mesoproterozoic Lakhanda shales in southeastern Yakutia, Russia: implications for mineralogical and provenance control, and recycling. Precambr. Res. 104 (1–2), 77–93. https://doi.org/10.1016/S0301-9268(00)00090-5.

Dettman, D.L., Fang, X., Garzione, C.N., Li, J., 2003. Uplift-driven climate change at 12 Ma: a long δ18O record from the NE margin of the Tibetan plateau. Earth Planet. Sci. Lett. 214 (1–2), 267–277. https://doi.org/10.1016/S0012-821X(03)00383-2.

Dickinson, W.R., 1985. Interpreting provenance relations from detrital modes of sandstones. Provenance of arenites. Springer, Dordrecht, 333–361. DOI: 10.1007/978-94-017-2809-6_15.

Dickinson, W.R., Suczek, C.A., 1979. Plate tectonics and sandstone compositions. AAPG Bull. 63 (12), 2164–2182. https://doi.org/10.1306/2F9188FB-16CE-11D7-8645000102C1865D.

Dixon, J.L., Hartshorn, A.S., Heimsath, A.M., DiBiase, R.A., Whipple, K.X., 2012. Chemical weathering response to tectonic forcing: A soils perspective from the San Gabriel Mountains, California. Earth Planet. Sci. Lett. 323, 40–49. https://doi.org/10.1016/j.epsl.2012.01.010.

Duvall, A.R., Clark, M.K., Kirby, E., Farley, K.A., Craddock, W.H., Li, C., Yuan, D.Y., 2013. Low-temperature thermochronometry along the Kunlun and Haiyuan Faults, NE Tibetan Plateau: Evidence for kinematic change during late-stage orogenesis. Tectonics 32 (5), 1190–1211. https://doi.org/10.1002/tect.20072.

Duzgoren-Aydin, N.S., Aydin, A., Malpas, J., 2002. Re-assessment of chemical weathering indices: case study on pyroclastic rocks of Hong Kong. Eng. Geol. 63 (1–2), 99–119. https://doi.org/10.1016/S0013-7952(01)00073-4.

Dypvik, H., Riber, L., Burca, F., Rüther, D., Jargvoll, D., Nagy, J., Jochmann, M., 2011. The Paleocene-Eocene thermal maximum (PETM) in Svalbard—clay mineral and geochemical signals. Palaeogeogr. Palaeoclimatol. Palaeoecol. 302 (3–4), 156–169. https://doi.org/10.1016/j.palaeo.2010.12.025.

Ehrmann, W., 1998. Implications of late Eocene to early Miocene clay mineral assemblages in McMurdo Sound (Ross Sea, Antarctica) on paleoclimate and ice dynamics. Palaeogeogr. Palaeoclimatol. Palaeoecol. 139 (3–4), 213–231. https://doi.org/10.1016/S0031-0182(97)00138-7.

Esquevin, J., 1969. Influence de la composition chimique des illites sur leur cristallinité. Bull. Centre Rech. Pau-SNPA 3 (1), 147–153.

Fang, X., Galy, A., Yang, Y., Zhang, W., Ye, C., Song, C., 2019. Paleogene global cooling–induced temperature feedback on chemical weathering, as recorded in the northern Tibetan Plateau. Geology 47 (10), 992–996. https://doi.org/10.1130/G46422.1.

Fang, X., Liu, D., Song, C., Dai, S., Meng, Q., 2013. Oligocene slow and Miocene-Quaternary rapid deformation and uplift of the Yumu Shan and North Qilian Shan: evidence from high-resolution magnetostratigraphy and tectonosedimentology. Geol. Soc., London, Spec. Publ. 373 (1), 149–171. https://doi.org/10.1144/SP373.5.

Fang, X., Wang, J., Zhang, W., Zan, J., Song, C., Yan, M., Appel, E., Zhang, T., Wu, F., Yang, Y., Lu, Y., 2016. Tectonosedimentary evolution model of an intracontinental flexural (foreland) basin for paleoclimatic research. Global Planet. Change 145, 78–97. https://doi.org/10.1016/j.gloplacha.2016.08.015.

Fang, X., Zhang, W., Meng, Q., Gao, J., Wang, X., King, J., Song, C., Dai, S., Miao, Y., 2007. High-resolution magnetostratigraphy of the Neogene Huaitoutala section in the eastern Qaidam Basin on the NE Tibetan Plateau, Qinghai Province, China and its implication on tectonic uplift of the NE Tibetan Plateau. Earth Planet. Sci. Lett. 258 (1–2), 293–306. https://doi.org/10.1016/j.epsl.2007.03.042.

Fathy, D., Wagreich, M., Zaki, R., Mohamed, R.S.A., Gier, S., Tyrrell, S., 2018. Geochemical fingerprinting of Maastrichtian oil shales from the Central Eastern Desert, Egypt: Implications for provenance, tectonic setting, and source area weathering. Geol. J. 53 (6), 2597–2612. https://doi.org/10.1002/gj.v53.610.1002/gj.3094.

Fedo, C.M., Nesbitt, H.W., Young, G.M., 1995. Unraveling the effects of potassium metasomatism in sedimentary rocks and paleosols, with implications for paleoweathering conditions and provenance. Geology 23 (10), 921–924. https://doi.org/10.1130/0091-7613(1995)023<0921:UTEOPM>2.3.CO;2.

Ferrier, K.L., Riebe, C.S., Jesse Hahm, W., 2016. Testing for supply-limited and kinetic-limited chemical erosion in field measurements of regolith production and chemical depletion. Geochem. Geophys. Geosyst. 17 (6), 2270–2285. https://doi.org/10.1002/ggge.v17.610.1002/2016GC006273.

Filippelli, G.M., 1997. Intensification of the Asian monsoon and a chemical weathering event in the late Miocene–early Pliocene: implications for late Neogene climate change. Geology 25 (1), 27–30. https://doi.org/10.1130/0091-7613(1997)025<0027:IOTAMA>2.3.CO;2.

Gabet, E.J., Mudd, S.M., 2009. A theoretical model coupling chemical weathering rates with denudation rates. Geology 37 (2), 151–154. https://doi.org/10.1130/G25270A.1.

Gao, P., Nie, J., Yan, Q., Zhang, X.u., Liu, Q., Cao, B.o., Pan, B., 2021. Millennial resolution late Miocene northern China precipitation record spanning astronomical analogue interval to the future. Geophys. Res. Lett. 48 (15) https://doi.org/10.1029/2021GL093942.

Garzanti, E., Andó, S., France-Lanord, C., Censi, P., Vignola, P., Galy, V., Lupker, M., 2011. Mineralogical and chemical variability of fluvial sediments 2. Suspended-load silt (Ganga–Brahmaputra, Bangladesh). Earth Planet. Sci. Lett. 302 (1–2), 107–120. https://doi.org/10.1016/j.epsl.2010.11.043.

Garzanti, E., Andò, S., Padoan, M., Vezzoli, G., El Kammar, A., 2015. The modern Nile sediment system: Processes and products. Quat. Sci. Rev. 130, 9–56. https://doi.org/10.1016/j.quascirev.2015.07.011.

Garzanti, E., Padoan, M., Andò, S., Resentini, A., Vezzoli, G., Lustrino, M., 2013a. Weathering and relative durability of detrital minerals in equatorial climate: sand petrology and geochemistry in the East African Rift. J. Geol. 121 (6), 547–580. https://doi.org/10.1086/673259.

Garzanti, E., Padoan, M., Setti, M., Najman, Y., Peruta, L., Villa, I.M., 2013b. Weathering geochemistry and Sr-Nd fingerprints of equatorial upper Nile and Congo muds. Geochem. Geophys. Geosyst. 14 (2), 292–316. https://doi.org/10.1002/ggge.20060.

Ge, J., Dai, Y., Zhang, Z., Zhao, D., Li, Q., Zhang, Y., Yi, L., Wu, H., Oldfield, F., Guo, Z., 2013. Major changes in East Asian climate in the mid-Pliocene: Triggered by the uplift of the Tibetan Plateau or global cooling? J. Asian Earth Sci. 69, 48–59. https://doi.org/10.1016/j.jseaes.2012.10.009.

Gehrels, G., Kapp, P., DeCelles, P., Pullen, A., Blakey, R., Weislogel, A., Ding, L., Guynn, J., Martin, A., McQuarrie, N., Yin, A., 2011. Detrital zircon geochronology of pre-Tertiary strata in the Tibetan-Himalayan orogen. Tectonics 30 (5), n/a–n/a. https://doi.org/10.1029/2011TC002868.

Gehrels, G.E., Yin, A., Wang, X.F., 2003. Magmatic history of the northeastern Tibetan Plateau. J. Geophys. Res. 108 (B9), 1–14. https://doi.org/10.1029/2002JB001876.

Geng, H., Pan, B., Huang, B., Cao, B., Gao, H., 2017. The spatial distribution of precipitation and topography in the Qilian Shan Mountains, northeastern Tibetan Plateau. Geomorphology 297, 43–54. https://doi.org/10.1016/j.geomorph.2017.08.050.

Gingele, F.X., Müller, P.M., Schneider, R.R., 1998. Orbital forcing of freshwater input in the Zaire Fan area—clay mineral evidence from the last 200 kyr. Palaeogeogr. Palaeoclimatol. Palaeoecol. 138 (1–4), 17–26. https://doi.org/10.1016/S0031-0182(97)00121-1.

Godard, V., Pik, R., Lavé, J., Cattin, R., Tibari, B., de Sigoyer, J., Pubellier, M., Zhu, J., 2009. Late Cenozoic evolution of the central Longmen Shan, eastern Tibet: insight from (U-Th)/He thermochronometry. Tectonics 28 (5), n/a–n/a. https://doi.org/10.1029/2008TC002407.

Godet, A., Bodin, S., Adatte, T., Föllmi, K.B., 2008. Platform-induced clay-mineral fractionation along a northern Tethyan basin-platform transect: implications for the interpretation of Early Cretaceous climate change (Late Hauterivian-Early Aptian). Cretac. Res. 29 (5–6), 830–847. https://doi.org/10.1016/j.cretres.2008.05.028.

Graly, J.A., Humphrey, N.F., Landowski, C.M., Harper, J.T., 2014. Chemical weathering under the Greenland ice sheet. Geology 42 (6), 551–554. https://doi.org/10.1130/G35370.110.1130/2014192.

Guo, P., Liu, C., Yu, M., Ma, D., Wang, P., Wang, K., Mao, G., Zhang, Q., 2018a. Paleosalinity evolution of the Paleogene perennial Qaidam lake on the Tibetan Plateau: climatic vs. tectonic control. Int. J. Earth Sci. 107 (5), 1641–1656. https://doi.org/10.1007/s00531-017-1564-8.

Guo, Y., Yang, S., Su, N., Li, C., Yin, P., Wang, Z., 2018b. Revisiting the effects of hydrodynamic sorting and sedimentary recycling on chemical weathering indices. Geochim. Cosmochim. Acta 227, 48–63. https://doi.org/10.1016/j.gca.2018.02.015.

Guo, Z.T., Ruddiman, W.F., Hao, Q.Z., Wu, H.B., Qiao, Y.S., Zhu, R.X., Peng, S.Z., Wei, J. J., Yuan, B.Y., Liu, T.S., 2002. Onset of Asian desertification by 22 Myr ago inferred from loess deposits in China. Nature 416, 159–163. https://doi.org/10.1038/416159a.

Harnois, L., 1988. The CIW index: a new chemical index of weathering. Sed. Geol. 55 (3), 319–322. https://doi.org/10.1016/0037-0738(88)90137-6.

Harris, N., 2006. The elevation history of the Tibetan Plateau and its implications for the Asian monsoon. Palaeogeogr. Palaeoclimatol. Palaeoecol. 241 (1), 4–15. https://doi.org/10.1016/j.palaeo.2006.07.009.

He, P., Song, C., Wang, Y., Meng, Q., Chen, L., Yao, L., Huang, R., Feng, W., Chen, S., 2018. Cenozoic deformation history of the Qilian Shan (northeastern Tibetan Plateau) constrained by detrital apatite fission-track thermochronology in the northeastern Qaidam Basin. Tectonophysics 749, 1–11. https://doi.org/10.1016/j.tecto.2018.10.017.

Hong, D., Jian, X., Fu, L., Zhang, W., 2020. Garnet trace element geochemistry as a sediment provenance indicator: An example from the Qaidam basin, northern Tibet. Mar. Pet. Geol. 116, 104316. https://doi.org/10.1016/j.marpetgeo.2020.104316.

Hou, M., Zhuang, G., Wu, M., 2021. Isotopic fingerprints of mountain uplift and global cooling in paleoclimatic and paleoecological records from the northern Tibetan Plateau. Palaeogeogr. Palaeoclimatol. Palaeoecol. 578, 110578. https://doi.org/10.1016/j.palaeo.2021.110578.

Hough, B.G., Garzione, C.N., Wang, Z., Lease, R.O., Burbank, D.W., Yuan, D., 2011. Stable isotope evidence for topographic growth and basin segmentation: Implications for the evolution of the NE Tibetan Plateau. Bulletin 123 (1-2), 168–185. https://doi.org/10.1130/B30090.110.1130/2011048.

Hu, J., Ma, Y., Li, Z., Wu, Y.i., Gao, W., Peng, B.o., Wei, X., Liu, D., Li, S., 2019. Jurassic sediments geochemical constraints on provenance, weathering process, and palaeoclimate variation of the north margin of Qaidam Basin, north-eastern Tibetan Plateau. Geol. J. 55 (4), 3247–3257. https://doi.org/10.1002/gj.v55.410.1002/gj.3542.

Huang, X., Jiang, D., Dong, X., Yang, S., Su, B., Li, X., Tang, Z., Wang, Y., 2019. Northwestward migration of the northern edge of the East Asian summer monsoon during the mid-Pliocene warm period: Simulations and reconstructions. J. Geophys. Res.: Atmos. 124 (3), 1392–1404. https://doi.org/10.1029/2018JD028995.

Hubert, J.F., 1962. A Zircon-Tourmaline-Rutile Maturity Index and the Interdependence of the Composition of Heavy Mineral Assemblages with the Gross Composition and Texture of Sandstones. J. Sediment. Res. 32 (3), 440–450. https://doi.org/10.1306/74D70CE5-2B21-11D7-8648000102C1865D.

Hui, Z., Gowan, E.J., Hou, Z., Zhou, X., Ma, Y., Guo, Z., Zhang, J., 2021. Intensified fire activity induced by aridification facilitated Late Miocene C4 plant expansion in the northeastern Tibetan Plateau, China. Palaeogeogr. Palaeoclimatol. Palaeoecol. 573, 110437. https://doi.org/10.1016/j.palaeo.2021.110437.

Ji, J., Zhang, K., Clift, P.D., Zhuang, G., Song, B., Ke, X., Xu, Y., 2017. High-resolution magnetostratigraphic study of the Paleogene-Neogene strata in the Northern Qaidam Basin: Implications for the growth of the Northeastern Tibetan Plateau. Gondwana Res. 46, 141–155. https://doi.org/10.1016/j.gr.2017.02.015.

Jian, X., Guan, P., Fu, S.T., Zhang, D.W., Zhang, W., Zhang, Y.S., 2014. Miocene sedimentary environment and climate change in the northwestern Qaidam basin, northeastern Tibetan Plateau: Facies, biomarker and stable isotopic evidences. Palaeogeogr. Palaeoclimatol. Palaeoecol. 414, 320–331. https://doi.org/10.1016/j.palaeo.2014.09.011.

Jian, X., Guan, P., Zhang, D.W., Zhang, W., Feng, F., Liu, R.J., Lin, S.D., 2013a. Provenance of Tertiary sandstone in the northern Qaidam basin, northeastern Tibetan Plateau: Integration of framework petrography, heavy mineral analysis and mineral chemistry. Sed. Geol. 290, 109–125. https://doi.org/10.1016/j.sedgeo.2013.03.010.

Jian, X., Guan, P., Zhang, W., Feng, F., 2013b. Geochemistry of Mesozoic and Cenozoic sediments in the northern Qaidam basin, northeastern Tibetan Plateau: implications for provenance and weathering. Chem. Geol. 360, 74–88. https://doi.org/10.1016/j.chemgeo.2013.10.011.

Jian, X., Guan, P., Zhang, W., Liang, H., Feng, F., Fu, L., 2018. Late Cretaceous to early Eocene deformation in the northern Tibetan Plateau: Detrital apatite fission track evidence from northern Qaidam basin. Gondwana Res. 60, 94–104. https://doi.org/10.1016/j.gr.2018.04.007.

Jian, X., Yang, S., Hong, D., Liang, H., Zhang, S., Fu, H., Zhang, W., 2020a. Seasonal geochemical heterogeneity of sediments from a subtropical mountainous river in SE China. Mar. Geol. 422, 106120. https://doi.org/10.1016/j.margeo.2020.106120.

Jian, X., Weislogel, A., Pullen, A., Shang, F., 2020b. Formation and evolution of the Eastern Kunlun Range, northern Tibet: Evidence from detrital zircon U-Pb geochronology and Hf isotopes. Gondwana Res. 83, 63–79. https://doi.org/10.1016/j.gr.2020.01.015.

Jian, X., Zhang, W., Liang, H., Guan, P., Fu, L., 2019. Mineralogy, petrography and geochemistry of an early Eocene weathering profile on basement granodiorite of Qaidam basin, northern Tibet: Tectonic and paleoclimatic implications. Catena 172, 54–64. https://doi.org/10.1016/j.catena.2018.07.029.

Jolivet, M., Brunel, M., Seward, D., Xu, Z., Yang, J., Roger, F., Tapponnier, P., Malavieille, J., Arnaud, N., Wu, C., 2001. Mesozoic and Cenozoic tectonics of the northern edge of the Tibetan plateau: fission-track constraints. Tectonophysics 343 (1-2), 111–134. https://doi.org/10.1016/S0040-1951(01)00196-2.

Kamp, P.C., 2010. Arkose, subarkose, quartz sand, and associated muds derived from felsic plutonic rocks in glacial to tropical humid climates. J. Sediment. Res. 80 (10), 895–918. https://doi.org/10.2110/jsr.2010.081.

Kapp, P., DeCelles, P.G., Gehrels, G.E., Heizler, M., Ding, L., 2007. Geological records of the Lhasa-Qiangtang and Indo-Asian collisions in the Nima area of central Tibet. Geol. Soc. Am. Bull. 119 (7-8), 917–933. https://doi.org/10.1130/B26033.110.1130/2007166.

Kasting, J.F., 2019. The Goldilocks planet? How silicate weathering maintains Earth "just right". Elements: Int. Mag. Mineral., Geochem., Petrol. 15 (4), 235–240. https://doi.org/10.2138/gselements.15.4.235.

Kent-Corson, M.L., Ritts, B.D., Zhuang, G., Bovet, P.M., Graham, S.A., Chamberlain, C.P., 2009. Stable isotopic constraints on the tectonic, topographic, and climatic evolution of the northern margin of the Tibetan Plateau. Earth Planet. Sci. Lett. 282 (1–4), 158–166. https://doi.org/10.1016/j.epsl.2009.03.011.

Kirby, E., Reiners, P.W., Krol, M.A., Whipple, K.X., Hodges, K.V., Farley, K.A., Tang, W., Chen, Z., 2002. Late Cenozoic evolution of the eastern margin of the Tibetan Plateau: Inferences from 40Ar/39Ar and (U-Th)/He thermochronology. Tectonics 21 (1), 1–20. https://doi.org/10.1029/2000TC001246.

Koutsodendris, A., Allstädt, F.J., Kern, O.A., Kousis, I., Schwarz, F., Vannacci, M., Woutersen, A., Appel, E., Berke, M.A., Fang, X.M., Friedrich, O., Hoorn, C., Salzmann, U., Pross, J., 2019. Late Pliocene vegetation turnover on the NE Tibetan Plateau (Central Asia) triggered by early Northern Hemisphere glaciation. Global Planet. Change 180, 117–125. https://doi.org/10.1016/j.gloplacha.2019.06.001.

Kump, L.R., Brantley, S.L., Arthur, M.A., 2000. Chemical weathering, atmospheric CO2, and climate. Annu. Rev. Earth Planet. Sci. 28 (1), 611–667. https://doi.org/10.1146/annurev.earth.28.1.611.

Lease, R.O., Burbank, D.W., Gehrels, G.E., Wang, Z., Yuan, D., 2007. Signatures of mountain building: Detrital zircon U/Pb ages from northeastern Tibet. Geology 35 (3), 239–242. https://doi.org/10.1130/G23057A.1.

Lease, R.O., Burbank, D.W., Hough, B., Wang, Z., Yuan, D., 2012. Middle Miocene reorganization of deformation along the northeastern Tibetan Plateau. Geology, 39 (4): 359–362. DOI: 10.1130/G31356.1.

Li, B., Zuza, A.V., Chen, X., Hu, D., Shao, Z., Qi, B., Wang, Z.-Z., Levy, D.A., Xiong, X., 2020. Cenozoic multi-phase deformation in the Qilian Shan and out-of-sequence development of the northern Tibetan Plateau. Tectonophysics 782-783, 228423. https://doi.org/10.1016/j.tecto.2020.228423.

Li, C., Yang, S., 2010. Is chemical index of alteration (CIA) a reliable proxy for chemical weathering in global drainage basins? Am. J. Sci. 310 (2), 111–127. https://doi.org/10.2475/02.2010.03.

Li, J., Fang, X., Song, C., Pan, B., Ma, Y., Yan, M., 2014. Late Miocene-Quaternary rapid stepwise uplift of the NE Tibetan Plateau and its effects on climatic and environmental changes. Quat. Res. 81 (3), 400–423. https://doi.org/10.1016/j.yqres.2014.01.002.

Li, L., Garzione, C.N., Pullen, A., Chang, H., 2016. Early–middle Miocene topographic growth of the northern Tibetan Plateau: Stable isotope and sedimentation evidence from the southwestern Qaidam basin. Palaeogeogr. Palaeoclimatol. Palaeoecol. 461, 201–213. https://doi.org/10.1016/j.palaeo.2016.08.025.

Li, L.L., Wu, C.D., Fan, C.F., Li, J.J., Zhang, C.H., 2017. Carbon and oxygen isotopic constraints on paleoclimate and paleoelevation of the southwestern Qaidam basin, northern Tibetan Plateau. Geosci. Front. 8 (5), 1175–1186. https://doi.org/10.1016/j.gsf.2016.12.001.

Li, M., Tang, L., Yuan, W., 2015. Middle Miocene-Pliocene activities of the North Altyn fault system: evidence from apatite fission track data. Arabian J. Geosci. 8 (11), 9043–9054. https://doi.org/10.1007/s12517-015-1873-9.

Li, S.F., Valdes, P.J., Farnsworth, A., Davies-Barnard, T., Su, T., Lunt, D.J., Spicer, R.A., Liu, J., Deng, W., Huang, J., Tang, H., Ridgwell, A., Chen, L.L., Zhou, Z.K., 2021. Orographic evolution of northern Tibet shaped vegetation and plant diversity in eastern Asia. Sci. Adv. 7 (5), eabc7741. https://doi.org/10.1126/sciadv.abc7741.

Li, G., Pettke, T., Chen, J., 2011. Increasing Nd isotopic ratio of Asian dust indicates progressive uplift of the north Tibetan Plateau since the middle Miocene. Geology 39 (3), 199–202. https://doi.org/10.1130/G31734.110.1130/2011082.

Liu, X., Dong, B., Yin, Z.Y., Smith, R.S., Guo, Q., 2017. Continental drift and plateau uplift control origination and evolution of Asian and Australian monsoons. Sci. Rep. 7, 40344. https://doi.org/10.1038/srep40344.

Liu, X., Sun, H., Miao, Y., Dong, B., Yin, Z.Y., 2015. Impacts of uplift of northern Tibetan Plateau and formation of Asian inland deserts on regional climate and environment. Quat. Sci. Rev. 116, 1–14. https://doi.org/10.1016/j.quascirev.2015.03.010.

Liu, Y., Song, C., Meng, Q., He, P., Yang, R., Huang, R., Chen, S., Wang, D., Xing, Z., 2020. Paleoclimate change since the Miocene inferred from clay-mineral records of the Jiuquan Basin, NW China. Palaeogeogr. Palaeoclimatol. Palaeoecol. 550, 109730. https://doi.org/10.1016/j.palaeo.2020.109730.

Liu, Y.J., Neubauer, F., Genser, J., Ge, X.H., Takasu, A., Yuan, S.H., Chang, L., Li, W.M., 2007a. Geochronology of the initiation and displacement of the Altyn Strike-Slip Fault, western China. J. Asian Earth Sci. 29 (2–3), 243–252. https://doi.org/10.1016/j.jseaes.2006.03.002.

Liu, Z., Colin, C., Huang, W., Le, K.P., Tong, S., Chen, Z., Trentesaux, A., 2007b. Climatic and tectonic controls on weathering in south China and Indochina Peninsula: Clay mineralogical and geochemical investigations from the Pearl, Red, and Mekong drainage basins. Geochem. Geophys. Geosyst. 8 (5), 1–18. https://doi.org/10.1029/2006GC001490.

Liu, Z., Tuo, S., Colin, C., Liu, J.T., Huang, C.Y., Selvaraj, K., Chen, C., Zhao, Y., Siringan, F.P., Boulay, S., Chen, Z., 2008. Detrital fine-grained sediment contribution from Taiwan to the northern South China Sea and its relation to regional ocean circulation. Mar. Geol. 255 (3–4), 149–155. https://doi.org/10.1016/j.margeo.2008.08.003.

Liu, Z., Wang, H., Hantoro, W.S., Sathiamurthy, E., Colin, C., Zhao, Y., Li, J., 2012. Climatic and tectonic controls on chemical weathering in tropical Southeast Asia (Malay Peninsula, Borneo, and Sumatra). Chem. Geol. 291, 1–12. https://doi.org/10.1016/j.chemgeo.2011.11.015.

Liu, Z., Zhao, Y., Colin, C., Siringan, F.P., Wu, Q., 2009. Chemical weathering in Luzon, Philippines from clay mineralogy and major-element geochemistry of river sediments. Appl. Geochem. 24 (11), 2195–2205. https://doi.org/10.1016/j.apgeochem.2009.09.025.

Liu-Zeng, J., Tapponnier, P., Gaudemer, Y., Ding, L., 2008. Quantifying landscape differences across the Tibetan plateau: Implications for topographic relief evolution. J. Geophys. Res. Earth Surf. 113 (F4), 1–26. https://doi.org/10.1029/2007JF000897.

Lu, F., An, Z., Chang, H., Dodson, J., Qiang, X., Yan, H., Dong, J., Song, Y., Fu, C., Li, X., 2017. Climate change and tectonic activity during the early Pliocene Warm Period from the ostracod record at Lake Qinghai, northeastern Tibetan Plateau. J. Asian Earth Sci. 138, 466–476. https://doi.org/10.1016/j.jseaes.2017.02.031.

Lu, H., Wang, E., Meng, K., 2014. Paleomagnetism and anisotropy of magnetic susceptibility of the Tertiary Janggalsay section (southeast Tarim basin): Implications for Miocene tectonic evolution of the Altyn Tagh Range. Tectonophysics 618, 67–78. https://doi.org/10.1016/j.tecto.2014.01.031.

Lu, H., Xiong, S., 2009. Magnetostratigraphy of the Dahonggou section, northern Qaidam Basin and its bearing on Cenozoic tectonic evolution of the Qilian Shan and Altyn Tagh Fault. Earth Planet. Sci. Lett. 288 (3–4), 539–550. https://doi.org/10.1016/j.epsl.2009.10.016.

Lu, H., Ye, J., Guo, L., Pan, J., Xiong, S., Li, H., 2019. Towards a clarification of the provenance of Cenozoic sediments in the northern Qaidam Basin. Lithosphere 11 (2), 252–272. https://doi.org/10.1130/L1037.1.

Lu, Y., Dewald, N., Koutsodendris, A., Kaboth-Bahr, S., Rösler, W., Fang, X., Pross, J., Appel, E., Friedrich, O., 2020. Sedimentological evidence for pronounced glacial-interglacial climate fluctuations in NE Tibet in the latest Pliocene to early Pleistocene. Paleoceanogr. Paleoclimatol. 35(5): e2020PA003864. DOI: 10.1029/2020PA003864.

Ma, X., Jiang, H., 2015. Combined tectonics and climate forcing for the widespread aeolian dust accumulation in the Chinese Loess Plateau since the early late Miocene. Int. Geol. Rev. 57 (14), 1861–1876. https://doi.org/10.1080/00206814.2015.1027305.

Maher, K., Chamberlain, C.P., 2014. Hydrologic regulation of chemical weathering and the geologic carbon cycle. Science 343 (6178), 1502–1504. https://doi.org/10.1126/science.1250770.

Mao, L., Xiao, A., Wu, L., Li, B., Wang, L., Lou, Q., Dong, Y., Qin, S., 2014. Cenozoic tectonic and sedimentary evolution of southern Qaidam Basin, NE Tibetan Plateau and its implication for the rejuvenation of Eastern Kunlun Mountains. Science China Earth Sciences 57 (11), 2726–2739. https://doi.org/10.1007/s11430-014-4951-z.

McLennan, S.M., 1989. Rare earth elements in sedimentary rocks: influence of provenance and sedimentary processes. Geochemistry and Mineralogy of Rare Earth Elements, Reviews in Mineralogy 21, Chapter 7: 169–200.

McLennan, S.M., 1993. Weathering and global denudation. J. Geol. 101 (2), 295–303. https://doi.org/10.1086/648222.

Mei, H., Jian, X., Zhang, W., Fu, H., Zhang, S., 2021. Behavioral differences between weathering and pedogenesis in a subtropical humid granitic terrain: Implications for chemical weathering intensity evaluation. Catena 203, 105368. https://doi.org/10.1016/j.catena.2021.105368.

Meng, Q., Song, C., Nie, J., Liu, C., He, P., Liu, F., Li, L., 2020. Middle-late Miocene rapid exhumation of the southern Qilian Shan and implications for propagation of the Tibetan Plateau. Tectonophysics 774, 228279. https://doi.org/10.1016/j.tecto.2019.228279.

Menold, C.A., Grove, M., Manning, C.E., Yin, A., Young, E.D., Ziegler, K., 2016. Argon and oxygen isotopic evidence for pervasive metasomatism during ultrahigh-pressure continental subduction. Earth Planet. Sci. Lett. 446, 56–67.

Miao, W., Fan, Q., Wei, H., Zhang, X., Ma, H., 2016a. Clay mineralogical and geochemical constraints on late Pleistocene weathering processes of the Qaidam Basin, northern Tibetan Plateau. J. Asian Earth Sci. 127, 267–280. https://doi.org/10.1016/j.jseaes.2016.06.013.

Miao, Y., Herrmann, M., Wu, F., Yan, X., Yang, S., 2012. What controlled Mid-Late Miocene long-term aridification in Central Asia? — Global cooling or Tibetan Plateau uplift: A review. Earth Sci. Rev. 112 (3–4), 155–172. https://doi.org/10.1016/j.earscirev.2012.02.003.

Miao, Y., Song, C., Fang, X., Meng, Q., Zhang, P., Wu, F., Yan, X., 2016b. Late Cenozoic genus Fupingopollenites development and its implications for the Asian summer monsoon evolution. Gondwana Res. 29 (1), 320–333. https://doi.org/10.1016/j.gr.2014.12.007.

Miao, Y., Wu, F., Warny, S., Fang, X., Lu, H., Fu, B., Song, C., Yan, X., Escarguel, G., Yang, Y., Meng, Q., Shi, P., 2019. Miocene fire intensification linked to continuous aridification on the Tibetan Plateau. Geology 47 (4), 303–307. https://doi.org/10.1130/G45720.1.

Miao, Y.F., Fang, X.M., Wu, F.L., Cai, M.T., Song, C.H., Meng, Q.Q., Xu, L., 2013. Late Cenozoic continuous aridification in the western Qaidam Basin: evidence from sporopollen records. Clim. Past 9 (4), 1863–1877. https://doi.org/10.5194/cp-9-1863-2013.

Mo, X.X., Luo, Z.H., Deng, J.F., Yu, X.H., Liu, C.D., Chen, H.W., Yuan, W.M., Liu, Y.H., 2007. Granitoids and crustal growth in the East-Kunlun orogenic belt. Geol. J. China Univ. 13 (3), 403–414.

Moore, D.M., Reynolds, R.C., 1997. X-ray Diffraction and the Identification and Analysis of Clay Minerals, second edition. Oxford University Press, New York.

Mutz, S.G., Ehlers, T.A., Werner, M., Lohmann, G., Stepanek, C., Li, J., 2018. Estimates of late Cenozoic climate change relevant to Earth surface processes in tectonically active orogens. Earth Surf. Dyn. 6 (2), 271–301. https://doi.org/10.5194/esurf-6-271-2018.

Nesbitt, H.W., Young, G.M., 1982. Early Proterozoic climates and plate motions inferred from major element chemistry of lutites. Nature 299 (5885), 715–717. https://doi.org/10.1038/299715a0.

Nesbitt, H.W., Young, G.M., 1984. Prediction of some weathering trends of plutonic and volcanic rocks based on thermodynamic and kinetic considerations. Geochim. Cosmochim. Acta 48 (7), 1523–1534. https://doi.org/10.1016/0016-7037(84)90408-3.

Nesbitt, H.W., Young, G.M., McLennan, S.M., Keays, R.R., 1996. Effects of chemical weathering and sorting on the petrogenesis of siliciclastic sediments, with implications for provenance studies. J. Geol. 104 (5), 525–542. https://doi.org/10.1086/629850.

Nie, J., Garzione, C., Su, Q., Liu, Q., Zhang, R., Heslop, D., Necula, C., Zhang, S., Song, Y., Luo, Z., 2017. Dominant 100,000-year precipitation cyclicity in a late Miocene lake from northeast Tibet. Sci. Adv. 3 (3), e1600762 https://doi.org/10.1130/B35175.1.

Nie, J., Ren, X., Saylor, J.E., Su, Q., Horton, B.K., Bush, M.A., Chen, W., Pfaff, K., 2020. Magnetic polarity stratigraphy, provenance, and paleoclimate analysis of Cenozoic strata in the Qaidam Basin, NE Tibetan Plateau. Geol. Soc. Am. Bull. 132 (1–2), 310–320. https://doi.org/10.1130/B35175.1.

Oliva, P., Viers, J., Dupré, B., 2003. Chemical weathering in granitic environments. Chem. Geol. 202 (3–4), 225–256. https://doi.org/10.1016/j.chemgeo.2002.08.001.

Pang, J., Yu, J., Zheng, D., Wang, W., Ma, Y., Wang, Y., Li, C., Li, Y., Wang, Y., 2019. Neogene expansion of the Qilian Shan, north Tibet: Implications for the dynamic evolution of the Tibetan Plateau. Tectonics 38 (3), 1018–1032. https://doi.org/10.1029/2018TC005258.

Peng, Y., Zhang, Y., Sun, J., Xing, E., Yu, H., 2018. Geochemistry of Late Carboniferous sedimentary rocks from the Zongwulong structural belt and adjacent areas, Qaidam Basin, China: Implications for provenance and tectonic setting. Geosci. J. 22 (2), 287–301. https://doi.org/10.1007/s12303-017-0032-6.

Penman, D.E., Caves Rugenstein, J.K., Ibarra, D.E., Winnick, M.J., 2020. Silicate weathering as a feedback and forcing in Earth's climate and carbon cycle. Earth Sci. Rev. 209, 103298. https://doi.org/10.1016/j.earscirev.2020.103298.

Perri, F., 2018. Reconstructing chemical weathering during the Lower Mesozoic in the Western-Central Mediterranean area: a review of geochemical proxies. Geol. Mag. 155 (4), 944–954. https://doi.org/10.1017/S0016756816001205.

Qi, B., Hu, D., Yang, X., Zhang, X., Zhao, X., 2015. Paleoelevation of the Qilian Mountain Inferred from Carbon and Oxygen Isotopes of Cenozoic Strata. Acta Geosci. Sinica (in Chinese) 36 (3), 323–332. https://doi.org/10.3975/cagsb.2015.03.07.

Rasmussen, C., Brantley, S., Richter, D.D., Blum, A., Dixon, J., White, A.F., 2011. Strong climate and tectonic control on plagioclase weathering in granitic terrain. Earth Planet. Sci. Lett. 301 (3–4), 521–530. https://doi.org/10.1016/j.epsl.2010.11.037.

Raymo, M.E., Ruddiman, W.F., 1992. Tectonic forcing of late Cenozoic climate. Nature 359 (6391), 117–122. https://doi.org/10.1038/359117a0.

Ren, X., Nie, J., Saylor, J.E., Li, H., Bush, M.A., Horton, B.K., 2019. Provenance Control on Chemical Weathering Index of Fluvio-Lacustrine Sediments: Evidence From the Qaidam Basin, NE Tibetan Plateau. Geochem. Geophys. Geosyst. 20 (7), 3216–3224. https://doi.org/10.1029/2019GC008330.

Ren, X., Nie, J., Saylor, J.E., Wang, X., Liu, F., Horton, B. K. 2020. Temperature control on silicate weathering intensity and evolution of the Neogene East Asian summer monsoon. Geophys. Res. Lett. 47(15): e2020GL088808. DOI: 10.1029/2020GL088808.

Riebe, C.S., Hahm, W.J., Brantley, S.L., 2017. Controls on deep critical zone architecture: A historical review and four testable hypotheses. Earth Surf. Proc. Land. 42 (1), 128–156. https://doi.org/10.1002/esp.v42.110.1002/esp.4052.

Riebe, C.S., Kirchner, J.W., Finkel, R.C., 2004. Erosional and climatic effects on long-term chemical weathering rates in granitic landscapes spanning diverse climate regimes. Earth Planet. Sci. Lett. 224 (3–4), 547–562. https://doi.org/10.1016/j.epsl.2004.05.019.

Rieu, R., Allen, P.A., Plotze, M., Pettke, T., 2007. Compositional and mineralogical variations in a Neoproterozoic glacially influenced succession, Mirbat area, south Oman: Implications for paleoweathering conditions. Precambr. Res. 154 (3–4), 248–265. https://doi.org/10.1016/j.precamres.2007.01.003.

Ritts, B.D., Biffi, U., 2001. Mesozoic northeast Qaidam basin: Response to contractional reactivation of the Qilian Shan, and implications for the extent of Mesozoic intracontinental deformation in central Asia. Geol. Soc. Am. 194, 293–316.

Ritts, B.D., Yue, Y., Graham, S.A., Sobel, E.R., Abbink, O.A., Stockli, D., 2008. From sea level to high elevation in 15 million years: Uplift history of the northern Tibetan Plateau margin in the Altun Shan. Am. J. Sci. 308 (5), 657–678. https://doi.org/10.2475/05.2008.01.

Roe, G.H., Montgomery, D.R., Hallet, B., 2003. Orographic precipitation and the relief of mountain ranges. J. Geophys. Res. Solid Earth 108 (B6), 2315. https://doi.org/10.1029/2001JB001521.

Roy, D.K., Roser, B.P., 2013. Climatic control on the composition of Carboniferous-Permian Gondwana sediments, Khalaspir basin, Bangladesh. Gondwana Res. 23 (3), 1163–1171. https://doi.org/10.1016/j.gr.2012.07.006.

Scarciglia, F., Le Pera, E., Critelli, S., 2005. Weathering and pedogenesis in the Sila Grande Massif (Calabria, South Italy): from field scale to micromorphology. Catena 61 (1), 1–29. https://doi.org/10.1016/j.catena.2005.02.001.

Scribner, C.A., Martin, E.E., Martin, J.B., Deuerling, K.M., Collazo, D.F., Marshall, A.T., 2015. Exposure age and climate controls on weathering in deglaciated watersheds of western Greenland. Geochim. Cosmochim. Acta 170, 157–172. https://doi.org/10.1016/j.gca.2015.08.008.

Selvaraj, K., Chen, C.T.A., 2006. Moderate chemical weathering of subtropical Taiwan: constraints from solid-phase geochemistry of sediments and sedimentary rocks. J. Geol. 114 (1), 101–116. https://doi.org/10.1086/498102.

Shao, J., Yang, S., Li, C., 2012. Chemical indices (CIA and WIP) as proxies for integrated chemical weathering in China: inferences from analysis of fluvial sediments. Sed. Geol. 265, 110–120. https://doi.org/10.1016/j.sedgeo.2012.03.020.

Shevenell, A.E., Kennett, J.P., Lea, D.W., 2004. Middle Miocene southern ocean cooling and Antarctic cryosphere expansion. Science 305 (5691), 1766–1770. https://doi.org/10.1126/science.1100061.

Shi, Z., Liu, X., An, Z., Yi, B., Yang, P., Mahowald, N., 2011. Simulated variations of eolian dust from inner Asian deserts at the mid-Pliocene, last glacial maximum, and present day: contributions from the regional tectonic uplift and global climate change. Clim. Dyn. 37 (11–12), 2289–2301. https://doi.org/10.1007/s00382-011-1078-1.

Song, B., Spicer, R.A., Zhang, K., Ji, J., Farnsworth, A., Hughes, A.C., Yang, Y., Han, F., Xu, Y., Spicer, T., Shen, T., Lunt, D.J., Shi, G., 2020. Qaidam Basin leaf fossils show northeastern Tibet was high, wet and cool in the early Oligocene. Earth Planet. Sci. Lett. 537, 116175. https://doi.org/10.1016/j.epsl.2020.116175.

Song, B., Zhang, K., Hou, Y., Ji, J., Wang, J., Yang, Y., Yang, T., Wang, C., Shen, T., 2019. New insights into the provenance of Cenozoic strata in the Qaidam Basin, northern Tibet: Constraints from combined U-Pb dating of detrital zircons in recent and ancient fluvial sediments. Palaeogeogr. Palaeoclimatol. Palaeoecol. 533, 109254. https://doi.org/10.1016/j.palaeo.2019.109254.

Song, B., Zhang, K., Zhang, L., Ji, J., Hong, H., Wei, Y., Xu, Y., Algeo, T., Wang, C., 2018a. Qaidam Basin paleosols reflect climate and weathering intensity on the northeastern Tibetan Plateau during the Early Eocene Climatic Optimum. Palaeogeogr. Palaeoclimatol. Palaeoecol. 512, 6–22. https://doi.org/10.1016/j.palaeo.2018.03.027.

Song, C., Hu, S., Han, W., Zhang, T., Fang, X., Gao, J., Wu, F., 2014. Middle Miocene to earliest Pliocene sedimentological and geochemical records of climate change in the western Qaidam Basin on the NE Tibetan Plateau. Palaeogeogr. Palaeoclimatol. Palaeoecol. 395, 67–76. https://doi.org/10.1016/j.palaeo.2013.12.022.

Song, Y., Wang, Q., An, Z., Qiang, X., Dong, J., Chang, H., Zhang, M., Guo, X., 2018b. Mid-Miocene climatic optimum: Clay mineral evidence from the red clay succession, Longzhong Basin, Northern China. Palaeogeogr. Palaeoclimatol. Palaeoecol. 512, 46–55. https://doi.org/10.1016/j.palaeo.2017.10.001.

Spicer, R.A., Harris, N.B., Widdowson, M., Herman, A.B., Guo, S., Valdes, P.J., Wolfe, J. A., Kelley, S.P., 2003. Constant elevation of southern Tibet over the past 15 million years. Nature 421 (6923), 622–624. https://doi.org/10.1038/nature01356.

Sun, J., Xu, Q., Liu, W., Zhang, Z., Xue, L., Zhao, P., 2014. Palynological evidence for the latest Oligocene– early Miocene paleoelevation estimate in the Lunpola Basin, central Tibet. Palaeogeogr. Palaeoclimatol. Palaeoecol. 399, 21–30. https://doi.org/10.1016/j.palaeo.2014.02.004.

Sun, J., Zhang, L., Deng, C., Zhu, R., 2008. Evidence for enhanced aridity in the Tarim Basin of China since 5.3 Ma. Quat. Sci. Rev. 27 (9–10), 1012–1023. https://doi.org/10.1016/j.quascirev.2008.01.011.

Sun, J.M., Liu, W.G., Liu, Z.H., Fu, B.H., 2017. Effects of the uplift of the Tibetan Plateau and retreat of Neotethys Ocean on the stepwise aridification of mid-latitude Asian Interior. Bull. Chin. Acad. Sci. 32 (9), 951–958.

Sun, M., Wu, W., Ji, X., Wang, X., Qu, S., 2019. Silicate weathering rate and its controlling factors: A study from small granitic watersheds in the Jiuhua Mountains. Chem. Geol. 504, 253–266. https://doi.org/10.1016/j.chemgeo.2018.11.019.

Sun, S.S., McDonough, W.F., 1989. Chemical and isotopic systematics of oceanic basalts: implications for mantle composition and processes. Geol. Soc., London, Spec. Publ. 42 (1), 313–345. https://doi.org/10.1144/GSL.SP.1989.042.01.19.

Sun, X., Wang, P., 2005. How old is the Asian monsoon system? Palaeobotanical records from China. Palaeogeogr. Palaeoclimatol. Palaeoecol. 222 (3-4), 181–222. https://doi.org/10.1016/j.palaeo.2005.03.005.

Sun, Y., Liu, J., Liang, Y.u., Ji, J., Liu, W., Aitchison, J.C., Sun, J., Lu, J., Song, B., Xu, Y., Zhang, K., Liu, Z., 2020. Cenozoic moisture fluctuations on the northeastern Tibetan Plateau and association with global climatic conditions. J. Asian Earth Sci. 200, 104490. https://doi.org/10.1016/j.jseaes.2020.104490.

Sun, Y., Ma, L., Bloemendal, J., Clemens, S., Qiang, X., An, Z., 2015. Miocene climate change on the Chinese Loess Plateau: Possible links to the growth of the northern Tibetan Plateau and global cooling. Geochem. Geophys. Geosyst. 16 (7), 2097–2108. https://doi.org/10.1002/2015GC005750.

Taylor, S.R., McLennan, S.M., 1985. The continental crust: its composition and evolution. Blackwell, London, pp. 312–315.

Wan, S., Clift, P.D., Li, A., Yu, Z., Li, T., Hu, D., 2012. Tectonic and climatic controls on long-term silicate weathering in Asia since 5 Ma. Geophys. Res. Lett. 39 (15) https://doi.org/10.1029/2012gl052377.

Wang, C., Adriaens, R., Hong, H., Elsen, J., Vandenberghe, N., Lourens, L.J., Gingerich, P. D., Abels, H.A., 2017a. Clay mineralogical constraints on weathering in response to early Eocene hyperthermal events in the Bighorn Basin, Wyoming (Western Interior, USA). Geol. Soc. Am. Bull. 129 (7-8), 997–1011. https://doi.org/10.1130/B31515.110.1130/2017140.

Wang, C., Dai, J., Zhao, X., Li, Y., Graham, S.A., He, D., Ran, B., Meng, J., 2014. Outward-growth of the Tibetan Plateau during the Cenozoic: A review. Tectonophysics 621, 1–43. https://doi.org/10.1016/j.tecto.2014.01.036.

Wang, C., Hong, H., Abels, H.A., Li, Z., Cao, K., Yin, K., Song, B., Xu, Y., Ji, J., Zhang, K., 2016. Early middle Miocene tectonic uplift of the northwestern part of the Qinghai-Tibetan Plateau evidenced by geochemical and mineralogical records in the western Tarim Basin. Int. J. Earth Sci. 105 (3), 1021–1037. https://doi.org/10.1007/s00531-015-1212-0.

Wang, E., Kirby, E., Furlong, K.P., Van Soest, M., Xu, G., Shi, X., Kamp, P.J.J., Hodges, K. V., 2012a. Two-phase growth of high topography in eastern Tibet during the Cenozoic. Nat. Geosci. 5 (9), 640–645. https://doi.org/10.1038/ngeo1538.

Wang, P., Du, Y., Yu, W., Algeo, T.J., Zhou, Q.i., Xu, Y., Qi, L., Yuan, L., Pan, W., 2020a. The chemical index of alteration (CIA) as a proxy for climate change during glacial-interglacial transitions in Earth history. Earth Sci. Rev. 201, 103032. https://doi.org/10.1016/j.earscirev.2019.103032.

Wang, Q., Song, Y., Li, Y., 2020b. Clay mineralogy of the upper Miocene-Pliocene red clay from the central Chinese Loess Plateau and its paleoclimate implications. Quat. Int. 552, 148–154. https://doi.org/10.1016/j.quaint.2019.11.039.

Wang, W., Zheng, D., Li, C., Wang, Y., Zhang, Z., Pang, J., Wang, Y., Yu, J., Wang, Y., Zheng, W., Zhang, H., Zhang, P., 2020c. Cenozoic exhumation of the Qilian Shan in the northeastern Tibetan Plateau: Evidence from low-temperature thermochronology. Tectonics 39 (4), e2019TC005705. https://doi.org/10.1029/2019TC005705.

Wang, W., Zhang, P., Wang, Z., Liu, K., Xu, H., Liu, C., Zhang, H., Zheng, W., Zheng, D., 2021. Multiproxy records in middle–late Miocene sediments from the Wushan Basin: Implications for climate change and tectonic deformation in the northeastern Tibetan Plateau. Geol. Soc. Am. Bull. 133 (1–2), 149–158. https://doi.org/10.1130/B35635.1.

Wang, W., Zheng, W., Zhang, P., Li, Q., Kirby, E., Yuan, D., Zheng, D., Liu, C., Wang, Z., Zhang, H., Pang, J., 2017b. Expansion of the Tibetan Plateau during the Neogene. Nat. Commun. 8 (1), 1–12. https://doi.org/10.1038/ncomms15887.

Wang, W.T., Zhang, P.Z., Kirby, E., Wang, L.H., Zhang, G.L., Zheng, D.W., Chai, C.Z., 2011. A revised chronology for Tertiary sedimentation in the Sikouzi basin: Implications for the tectonic evolution of the northeastern corner of the Tibetan Plateau. Tectonophysics 505 (1–4), 100–114. https://doi.org/10.1016/j.tecto.2011.04.006.

Wang, Y., Zheng, J., Zhang, W., Li, S., Liu, X., Yang, X., Liu, Y., 2012b. Cenozoic uplift of the Tibetan Plateau: Evidence from the tectonic–sedimentary evolution of the western Qaidam Basin. Geosci. Front. 3 (2), 175–187. https://doi.org/10.1016/j.gsf.2011.11.005.

West, A.J., Galy, A., Bickle, M., 2005. Tectonic and climatic controls on silicate weathering. Earth Planet. Sci. Lett. 235 (1–2), 211–228. https://doi.org/10.1016/j.epsl.2005.03.020.

Wu, L., Xiao, A., Wang, L., Shen, Z., Zhou, S., Chen, Y., Wang, L., Liu, D., Guan, J., 2011. Late Jurassic–early Cretaceous northern Qaidam basin, NW China: implications for the earliest Cretaceous intracontinental tectonism. Cretac. Res. 32 (4), 552–564. https://doi.org/10.1016/j.cretres.2011.04.002.

Xu, G., Kamp, P.J.J., 2000. Tectonics and denudation adjacent to the Xianshuihe Fault, eastern Tibetan Plateau: Constraints from fission track thermochronology. J. Geophys. Res. Solid Earth 105 (B8), 19231–19251. https://doi.org/10.1029/2000JB900159.

Xu, Z., Li, T., Wan, S., Nan, Q., Li, A., Chang, F., Jiang, F., Tang, Z., 2012. Evolution of East Asian monsoon: Clay mineral evidence in the western Philippine Sea over the past 700 kyr. J. Asian Earth Sci. 60, 188–196. https://doi.org/10.1016/j.jseaes.2012.08.018.

Yan, Z., Xiao, W.J., Windley, B.F., Wang, Z.Q., Li, J.L., 2010. Silurian clastic sediments in the North Qilian Shan, NW China: Chemical and isotopic constraints on their forearc provenance with implications for the Paleozoic evolution of the Tibetan Plateau. Sed. Geol. 231 (3–4), 98–114. https://doi.org/10.1016/j.sedgeo.2010.09.001.

Yang, J., Cawood, P.A., Montañez, I.P., Condon, D.J., Du, Y., Yan, J.-X., Yan, S., Yuan, D., 2020. Enhanced continental weathering and large igneous province induced climate warming at the Permo-Carboniferous transition. Earth Planet. Sci. Lett. 534, 116074. https://doi.org/10.1016/j.epsl.2020.116074.

Yang, R., Yang, Y., Fang, X., Ruan, X., Galy, A., Ye, C., Meng, Q., Han, W., 2019. Late Miocene intensified tectonic uplift and climatic aridification on the northeastern

Tibetan Plateau: Evidence from clay mineralogical and geochemical records in the Xining Basin. Geochem. Geophys. Geosyst. 20 (2), 829–851. https://doi.org/10.1029/2018GC007917.

Yang, W., Spiro, B., Guo, Z.-J., Pentecost, A., 2017. Cenozoic lacustrine stromatolites from the southern margin of the Junggar Basin, NW China and adjacent areas: indicators for palaeoclimatic and tectonic evolution. Geol. J. 52 (2), 249–262. https://doi.org/10.1002/gj.v52.210.1002/gj.2754.

Yang, Y., Fang, X., Galy, A., Jin, Z., Wu, F., Yang, R., Zhang, W., Zan, J., Liu, X., Gao, S., 2016. Plateau uplift forcing climate change around 8.6 Ma on the northeastern Tibetan Plateau: Evidence from an integrated sedimentary Sr record. Palaeogeogr. Palaeoclimatol. Palaeoecol. 461, 418–431. https://doi.org/10.1016/j.palaeo.2016.09.002.

Yin, A., Dang, Y.Q., Zhang, M., Chen, X.H., McRivette, M.W., 2008. Cenozoic tectonic evolution of the Qaidam basin and its surrounding regions (Part 3): Structural geology, sedimentation, and regional tectonic reconstruction. Geol. Soc. Am. Bull. 120 (7–8), 847–876. https://doi.org/10.1130/B26232.1.

Yin, A., Rumelhart, P.E., Butler, R., Cowgill, E., Harrison, T.M., Foster, D.A., Ingersoll, R. V., Zhang, Q., Zhou, X., Wang, X., Hanson, A., Raza, A., 2002. Tectonic history of the Altyn Tagh fault system in northern Tibet inferred from Cenozoic sedimentation. Geol. Soc. Am. Bull. 114 (10), 1257–1295. https://doi.org/10.1130/0016-7606(2002)114<1257:THOTAT>2.0.CO;2.

Yin, J., Zhang, S., Wu, Z., 2020. Provenance Analysis of the Paleogene Strata in the Northern Qaidam Basin, China: Evidences from Sediment Distribution, Heavy Mineral Assemblages and Detrital Zircon U-Pb Geochronology. Minerals 10 (10), 854. https://doi.org/10.3390/min10100854.

Yu, J., Zheng, D., Pang, J., Wang, Y., Fox, M., Vermeesch, P., Li, C., Xiao, L., Hao, Y., Wang, Y., 2019. Miocene Range Growth Along the Altyn Tagh Fault: Insights From Apatite Fission Track and (U-Th)/He Thermochronometry in the Western Danghenan Shan, China. J. Geophys. Res. Solid Earth 124 (8), 9433–9453. https://doi.org/10.1029/2019JB017570.

Yu, L., Xiao, A., Wu, L., Tian, Y., Rittner, M., Lou, Q., Pan, X., 2017. Provenance evolution of the Jurassic northern Qaidam Basin (West China) and its geological implications: evidence from detrital zircon geochronology. Int. J. Earth Sci. 106 (8), 2713–2726. https://doi.org/10.1007/s00531-017-1455-z.

Yu, X., Guo, Z., Chen, Y., Cheng, X., Du, W., Wang, Z., 2021. Recognition and application of offlap in endorheic basins: new insights into plateau growth. Int. Geol. Rev. 1–16 https://doi.org/10.1080/00206814.2021.1894611.

Yuan, D.-Y., Ge, W.-P., Chen, Z.-W., Li, C.-Y., Wang, Z.-C., Zhang, H.-P., Zhang, P.-Z., Zheng, D.-W., Zheng, W.-J., Craddock, W.H., Dayem, K.E., Duvall, A.R., Hough, B.G., Lease, R.O., Champagnac, J.-D., Burbank, D.W., Clark, M.K., Farley, K.A., Garzione, C.N., Kirby, E., Molnar, P., Roe, G.H., 2013. The growth of northeastern Tibet and its relevance to large-scale continental geodynamics: A review of recent studies. Tectonics 32 (5), 1358–1370. https://doi.org/10.1002/tect.v32.510.1002/tect.20081.

Zachos, J., Pagani, M., Sloan, L., Thomas, E., Billups, K., 2001. Trends, rhythms, and aberrations in global climate 65 Ma to present. Science 292 (5517), 686–693. https://doi.org/10.1126/science.1059412.

Zachos, J.C., Dickens, G.R., Zeebe, R.E., 2008. An early Cenozoic perspective on greenhouse warming and carbon-cycle dynamics. Nature 451 (7176), 279–283. https://doi.org/10.1038/nature06588.

Zan, J., Kang, J., Yan, M., Fang, X., Li, X., Guan, C., Zhang, W., Fang, Y., 2018. A pedogenic model for the magnetic enhancement of late Miocene fluvial-lacustrine sediments from the Xining Basin, NE Tibetan Plateau. J. Geophys. Res. Solid Earth 123 (8), 6176–6194. https://doi.org/10.1029/2018JB016064.

Zhai, L., Wu, C., Ye, Y., Zhang, S., Wang, Y., 2018. Fluctuations in chemical weathering on the Yangtze Block during the Ediacaran-Cambrian transition: implications for paleoclimatic conditions and the marine carbon cycle. Palaeogeogr. Palaeoclimatol. Palaeoecol. 490, 280–292. https://doi.org/10.1016/j.palaeo.2017.11.006.

Zhang, H., Zhang, P., Prush, V., Zheng, D., Zheng, W., Wang, W., Liu, C., Ren, Z., 2017. Tectonic geomorphology of the Qilian Shan in the northeastern Tibetan Plateau: Insights into the plateau formation processes. Tectonophysics 706, 103–115. https://doi.org/10.1016/j.tecto.2017.04.016.

Zhang, R., Jiang, D., Zhang, Z., Yu, E., 2015. The impact of regional uplift of the Tibetan Plateau on the Asian monsoon climate. Palaeogeogr. Palaeoclimatol. Palaeoecol. 417, 137–150. https://doi.org/10.1016/j.palaeo.2014.10.030.

Zhang, S., Jian, X., Pullen, A., Fu, L., Liang, H., Hong, D., Zhang, W., 2021a. Tectono-magmatic events of the Qilian orogenic belt in northern Tibet: new insights from detrital zircon geochronology of river sands. Int. Geol. Rev. 63 (8), 917–940. https://doi.org/10.1080/00206814.2020.1734876.

Zhang, T., Han, W., Fang, X., Miao, Y., Zhang, W., Song, C., Wang, Y., Khatri, D.B., Zhang, Z., 2018. Tectonic control of a change in sedimentary environment at~ 10 Ma in the northeastern Tibetan Plateau. Geophys. Res. Lett. 45 (14), 6843–6852. https://doi.org/10.1029/2018GL078460.

Zhang, T., Han, W., Fang, X., Song, C., Wang, Y., Tian, Q., Zhang, W., Feng, Z., Tan, M., 2021b. Tectonic forcing of environmental transition in Central Asia at~ 11–9 Ma. Gondwana Res. 89, 19–30. https://doi.org/10.1016/j.gr.2020.08.012.

Zhang, W., Zhang, H., Niu, J., Lei, G., Chang, F., 2020. Geochemical record of rapid climate change and chemical weathering in a semi-arid area, northeastern Tibetan Plateau. Geosci. J. 24 (6), 1–10. https://doi.org/10.1007/s12303-019-0049-0.

Zhang, Z.S., Wang, H., Guo, Z., Jiang, D., 2007. What triggers the transition of palaeoenvironmental patterns in China, the Tibetan Plateau uplift or the Paratethys Sea retreat? Palaeogeogr. Palaeoclimatol. Palaeoecol. 245 (3–4), 317–331. https://doi.org/10.1016/j.palaeo.2006.08.003.

Zhao, H., Qiang, X., Xu, X., Sun, Y., 2020. Iron oxide characteristics of the Chinese loess-red clay sequences and their implications for the evolution of the East Asian summer monsoon since the Late Oligocene. Palaeogeogr. Palaeoclimatol. Palaeoecol. 543, 109604. https://doi.org/10.1016/j.palaeo.2020.109604.

Zhao, M.Y., Zheng, Y.F., 2015. The intensity of chemical weathering: geochemical constraints from marine detrital sediments of Triassic age in South China. Chem. Geol. 391, 111–122. https://doi.org/10.1016/j.chemgeo.2014.11.004.

Zheng, D., Clark, M. K., Zhang, P., Zheng, W., Farley, K.A., 2010. Erosion, fault initiation and topographic growth of the North Qilian Shan (northern Tibetan Plateau). Geosphere, 6(6): 937–941. DOI: 10.1130/GES00523.1.

Zheng, D., Zhang, P.Z., Wan, J., Yuan, D., Li, C., Yin, G., Zhang, G., Wang, Z., Min, W., Chen, J., 2006. Rapid exhumation at~ 8 Ma on the Liupan Shan thrust fault from apatite fission-track thermochronology: Implications for growth of the northeastern Tibetan Plateau margin. Earth Planet. Sci. Lett. 248 (1–2), 198–208. https://doi.org/10.1016/j.epsl.2006.05.023.

Zhou, H., Chen, L., Diwu, C., Lei, C., Li, S., 2018. Cenozoic uplift of the Qimantage Mountains, northeastern Tibet: Contraints from provenance analysis of Cenozoic sediments in Qaidam Basin. Geol. J. 53 (6), 2613–2632. https://doi.org/10.1002/gj.v53.610.1002/gj.3095.

Zhu, W., Wu, C., Wang, J., Zhou, T., Li, J., Zhang, C., Li, L., 2017. Heavy mineral compositions and zircon U-Pb ages of Cenozoic sandstones in the SW Qaidam basin, northern Tibetan Plateau: Implications for provenance and tectonic setting. J. Asian Earth Sci. 146, 233–250. https://doi.org/10.1016/j.jseaes.2017.05.023.

Zhuang, G., Hourigan, J.K., Koch, P.L., Ritts, B.D., Kent-Corson, M.L., 2011a. Isotopic constraints on intensified aridity in Central Asia around 12 Ma. Earth Planet. Sci. Lett. 312 (1–2), 152–163. https://doi.org/10.1016/j.epsl.2011.10.005.

Zhuang, G., Hourigan, J.K., Ritts, B.D., Kent-Corson, M.L., 2011b. Cenozoic multiple-phase tectonic evolution of the northern Tibetan Plateau: Constraints from sedimentary records from Qaidam basin, Hexi Corridor, and Subei basin, northwest China. Am. J. Sci. 311 (2), 116–152. https://doi.org/10.2475/02.2011.02.

Zhuang, G., Johnstone, S.A., Hourigan, J., Ritts, B., Robinson, A., Sobel, E.R., 2018. Understanding the geologic evolution of Northern Tibetan Plateau with multiple thermochronometers. Gondwana Res. 58, 195–210. https://doi.org/10.1016/j.gr.2018.02.014.

Zhuang, G., Zhang, Y.G., Hourigan, J., Ritts, B., Hren, M., Hou, M., Wu, M., Kim, B., 2019. Microbial and geochronologic constraints on the Neogene paleotopography of northern Tibetan Plateau. Geophys. Res. Lett. 46 (3), 1312–1319. https://doi.org/10.1029/2018GL081505.